2021

Effects of Corrosion on the SERS Activity and Optical Response of Silver Nanorods

Christopher J. Mealer
University of North Florida, n00895292@unf.edu

“Effects of Corrosion on the SERS Activity and Optical Response of Silver Nanorods”

By

Christopher (C.J.) Mealer

A thesis submitted to the School of Engineering
in partial fulfillment of the requirements for the degree of
Master of Science in Mechanical Engineering
University of North Florida

COLLEGE OF COMPUTING, ENGINEERING, and CONSTRUCTION

April 2021

The thesis “Effects of Corrosion on the SERS Activity and Optical Response of Silver Nanorods” submitted by Christopher (C.J.) Mealer in partial fulfillment of the requirements for the degree of Master of Science in Mechanical Engineering has been

Approved by the thesis committee: **Date**

_____ _____

Dr. Stephen Stagon

Thesis Advisor and Committee Chairperson

_____ _____

Dr. Grant Bevill

_____ _____

Dr. Simsiriwong

Accepted for the School of Engineering:

_____ _____

Dr. Osama Jadaan

Director of the School of Engineering

Accepted for the College of Computing, Engineering, and Construction:

_____ _____

Dean Klostermeyer

Dean of the College

Accepted for the University:

_____ _____

Dr. John Kanter

Dean of the Graduate School

Dedication

This work is dedicated to Dr. Stagon, Mary and John Mealer, Coco Miller, and the Raman community. Although Shimadzu is nearly there, additionally, I'd like to dedicate this paper to Shimadzu Instruments, in helping their pursuit of becoming the greatest instrumentation maker in the world.

Christopher Mealer

Acknowledgements

First off, thank you Coco Miller for being the most supportive over the past 5 years. I couldn't have done it without you.

Tied for first, is Dr. Stagon. Thanks for helping me along this journey and making the best experience for me during graduate school. I truly believe this project had, and will continue to have, a significant impact for my career. I couldn't have done it without you.

Thank you Dr. Eason, I came to you for career advice and in a matter of two weeks, you changed my life dramatically.

Thank you Paul Rementer, my boss, for allowing me sufficient time to grow as a student and professional. I hope now, we can reap the benefits together!

Thank you Dean Klostermeyer for pushing me at times and getting me out of my comfort zone. Thank you for impacting my future in a highly positive way.

Thank you, Scott Curry, for the tremendous amount of career advice over the years. I enjoyed brainstorming and bouncing ideas off you every time. Thank you for always being so open to help.

UNF CCEC Dean staff Kathy, Carroll, Nida, Melody for all the support. Thank you for the advice and recommendation letters that allowed me to have two huge accomplishments, a university awards and a huge university fellowship for grad school. Thank you.

Thank you Dr. Murat, for mentoring and funding in the clubs I participated in and making me well rounded with a loaded resume.

Thank you Dr. Bevill and Dr. Simsiriwong, you both were always open for me to bounce ideas off. During undergrad and grad school you both positively impacted my technical abilities

Thank you, Dr. Schonning. Thank you for being a mentor and introducing me to "Rich Dad, Poor Dad."

Thank you Scott Zinn and Abbey Fraser, for the countless times I came to bounce thesis ideas and concepts off you. You were always their to help tackle anything I threw at you.

And last but not least, thank you Mom and Dad. I can't thank you enough for all the guidance over the years.

Table of Contents

List of Figures

List of Tables

Abstract

The nanoscience and nanotechnology community have a common goal in better understanding the surfaced enhanced Raman scattering (SERS) that occurs due to laser plasmon resonance in conjunction with metal enhanced substrates. Metallic nanostructures, such as silver (Ag) nanorods, are widely used in biological and chemical sensing applications that rely on the measurement of subtle changes in the optical response of the nanostructures in the presence of a target agent. The optical response of Ag nanorods and most other metallic nanostructures is highly sensitive to morphology and surface chemical termination. In pristine condition, the optical properties of Ag nanorods and other metallic nanostructures are well documented in the literature. However, almost nothing is known of the structure – property effects of exposure to solvents, buffered solutions, and similar in real applications. This document reports on the investigation into the effects of dissolved gasses, which are known to corrode bulk and thin film silver (Ag), in di-ionized water on Ag nanorods. Through SEM, SPM, UV-Vis, and Raman Spectroscopy, characterization of rapid corrosion and morphological changes are observed within minutes when Ag nanorods are exposed to water with dissolved gases present. Conversely, almost no measurable changes are observed when the dissolved gases are removed from the water via boiling. The current research attempts in exploiting the enhancement factors of optical properties dealing with SERS. Growing substrates to examine in SERS by using physical vapor deposition (PVD) on corning glass depositing Ag nanorods will enlighten the nanoscience and nanotechnology community on these changes in optical properties. SPM and SEM images both show significant differences through corrosion of Ag on the two different types of water. The species from corrosion in regular water appears to be AgO, as there is no Sulphur detected by the SEM's EDS spectrum. KFM shows clear differences in surface potential indicating a chemical change. UV-Vis shows a decrease in resonance and absorptivity after corroding. The goal of this investigation is to characterize oxidation species grown on the Ag nanorods when the substrate is exposed to H_2O and dissolved gasses. Raman Spectrum shows that for a fluorescent molecule (R6G), the overall measured Raman signal significantly increases with oxidation due to activation of surface enhanced fluorescence. Statistical T-test were run on spectrum, a value of 1.83E-05 was accessed to prove the significant increase in signal. When oxidation occurs from substrates stored in water with dissolved gases like the R6G samples, the scatter in the signal also significantly increases, proven with an f-test value of 4.76E-05. Additionally, when a non-resonant molecule is used, like our caffeine, the scatter in signal significantly increases, proven by f-test value of 2.4E-02. By experimenting contrasting substrate-samples during Raman that were taken straight out of vacuum or stored in water, the community can see the indicating affect measured in Raman spectra.

Keywords: Raman Spectroscopy, SERS, Surface Plasma Resonance (SPR), UV-Vis, SEM, Nanorods, Physical Vapor Deposition (PVD), Scanning Probe Microscopy (SPM), Kinetic Probe Force Microscopy (KFM)

Chapter 1. Introduction and Motivation

Surface enhanced Raman spectroscopy has become a hot topic of the 21st century. As the 2020's progress through the epidemic of COVID-19 with different severity of COVID strands, this has triggered interest by scientists in SERS because of its biosensing application for detecting diseases early on. By June 2020 8 million people around the world had been infected by COVID-19. The lifespan of this epidemic has been a little under a year now and the COVID virus has mutated several times and the current strand of January 2021 has become more contagious. [55] Can SERS contribute by applications in detecting COVID strands?

Throughout the 20th Century, and even early the 21st century, the nanoscience community is becoming larger and larger including literature being published throughout this trend. We have come to an era in which immense progress has been made in innovative instruments for analysis on the nanometer scale. These instruments have become commercially available by companies like Shimadzu for scientists to research with throughout the world. Their is significant room for further development and advancement on these nanoscale regimes of many technologies. Throughout the 20th century scientists have been analyzing and detecting early disease diagnostics by human biological fluids with Raman Spectroscopy. SERS substrates with surface plasmon resonance (SPR) such as silver nanorods grown on glass, has made possible detection of

amyloid beta for Alzheimer's disease [56], MiR-196ain for lung cancer [60], and many more early-on viruses have been analyzed.

SERS has the potential to enables time and cost efficiency over the current PCR testing to detect SARS-CoV-2 strand. PCR testing sometime can take hours and multiple cycles to test. This is where COVID-19 exposed time inefficiencies involving the PCR testing in turn resulting in the inability to diversify across clinical studies. [61] SERS in minutes yields a molecular finger print of the analyte under investigation. Not only is their room for improvement in polymerase chain reaction (PCR) testing involving time and cost, additionally improvements can be made in reliability and repeatability of testing. Reports have been made on the variability in results of testing the same patients. [61]

Raman Spectroscopy does not require large amounts of capital investments compared to other methods available. One of the main benefits to Raman spectroscopy is it does not require the analyte to include labels or markers. SERS can detect the intrinsic physical properties of the analyte purely. Labeling biomolecules can block binding sites degrading the detecting abilities of the subject. Due to the portability of Raman spectroscopy and low labor and time costs versus other methods, Raman analysis should be the preferred in lab-on-glass method for rapidly detecting many viruses in real time. An example of SERS sensitivity for detection was reported by the University of Cambridge that detection could be achieved of as little as 10^2 EID50/mL

(50% egg infective dose per microliter) with a virus specificity of 90% within minutes. [62] Additionally, SERS spectral graphs can monitor p24 antigen in blood plasma for HIV diagnosis with a 97.5% sensitivity and 95% specificity. [33]

Corrosion of Ag nanorod substrates is a huge issue concerning SERS. When substrates with metallic nanostructures are grown, the average diameter of each nanorod is approximately 200 nm, with the center to center spacing between each nanorod being approximately 100 nm. Furthermore, when the structure and spacing is this small, surface chemical reactions and morphological changes happen within minutes of being exposed to regular water or even air. The substrates can become compromised by oxidation and corrosion rapidly [40].

It is known in literature SERS enhancement is high when using Ag metallic nanostructure substrates. Studies suggest that the most likely cause for the decrease in SERS enhancement, while using Ag nanorods after storing these in air, is due to surface contamination of Sulfur and hydrocarbon fouling. [40] Before 21 days, the substrates signal to background ratio can vary by up to 20%. [40] Ag nanorod substrates for SERS stabilize from surface chemical changes and morphological changes after 21 days as shown in Figure 1. [40]

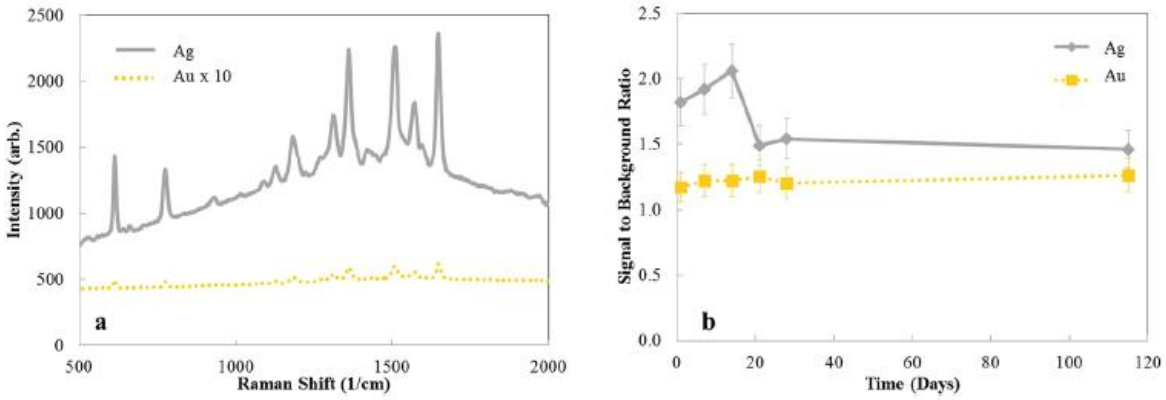

Figure 1: Recent studies show (a) Raman signal with R6G absorption on Ag and Au nanorod substrates and (b) signal to background ratio versus time over 4 months while perishing in air.

Literature suggests that the optical properties of metal thin film characterized by SERS is contributed from pinhole formations of corrosion. [43] The optical properties are not as much affected depending on the deposition techniques or the substrate used, but the SERS signals show significant degradation from when the samples are exposed to aqueous distilled water for relatively long periods of time. [43] Furthermore, 1 cm^2 samples exposed to distilled water for 24 hours were nearly stripped of all silver films. [43]

This creates irregularities for the repeatability later when detection tests are performed with the different substrates that have been sitting in relatively harsh environments. Herein lies the motivation behind this paper. This is an investigation in the corrosion and degrading issues with SERS biosensing substrates. This paper reports on how SERS samples exposed to regular water drive rapid surface corrosion, which is observed by an SPM image of topography differences after only 2 hours shown in Figure 2.

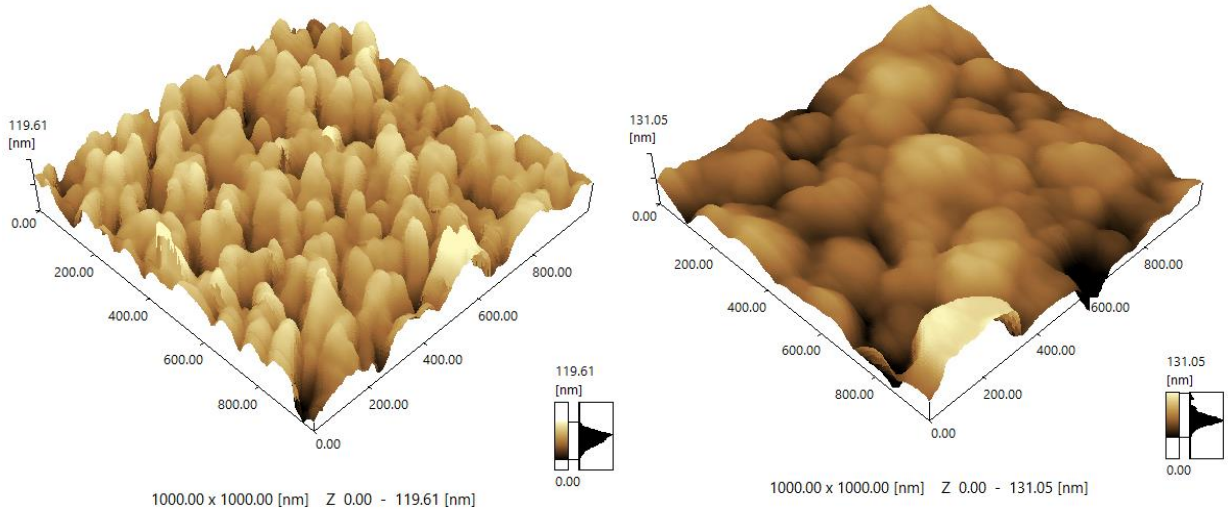

Figure 2: (Left) baseline Ag nanorods substrate straight out of vacuum topography versus (right) oxide perished Ag nanorods substrate after 2 hours in regular water.

This paper focuses on investigating corrosion of Ag nanorods in water, the most common way they are applied in sensing applications. Understanding this will dictate if substrates in experiments should be used in regular or degassed water. We hypothesize that it is the dissolved gases in water that are driving rapid surface corrosion and formations of silver oxide on silver nanorods. To characterize this oxide SEM, EDS, KFM, and UV-Vis are performed. Afterward, SERS experiments in the results section of this paper will be performed to show the significant changes in signal strength due to dissolved gasses in water. This paper will suggest on creating more reliable, repeatable, and longer lifespan of enhanced signal for detection using SERS biosensing metallic nanostructure substrates.

Chapter 2. Overview of Spectroscopy Methods

There are many Spectroscopy analysis tools used for identifying materials and molecules. These tools include Raman Spectroscopy, Fourier Transform Infrared Spectroscopy (FTIR), Near-Infrared Spectroscopy, ICP Emission, UV-Vis Spectroscopy, X-ray Fluorescence (XRF),

and Nuclear Magnetic Resonance (NMR) Spectroscopy. XRF and NMR in particular, focus in Atomic Spectroscopy to analyze chemical functional groups or specific atoms by sharp peaks in the spectra detected. XRF uses X-ray tubes to irradiate a sample, then the sample emits its own unique characteristic X-rays that are detected to understand elemental attributes. NMR uses radio waves onto nuclei magnetic fields for this atomic analysis. UV-Vis and FTIR are absorption spectroscopy using an excitation source of light, monochromatic or at different frequencies of light, are emitted on a sample to calculate the absorption of light by a sample. All these analyses are widely used and very useful in practice. Raman Spectroscopy is the main focus due to its ability to detect viruses. Raman uses a monochromatic laser to emit on a sample that changes the vibrational energy states of molecules. Raman relies on the inelastic scattering, known as Raman scattering, that leaves a molecular fingerprint of the specific molecule when the energy vibrational state is shift up or down. To understand Raman analysis, the latter of this section breaks the technique down into surface plasmon resonance created by the laser and surface enhanced Raman spectroscopy by the metallic substrates which influencing the spectral intensity.

Surface Plasmon Resonance (SPR)

SPR has emerged as a powerful optical detection technique to study biomolecular interaction in real time, food analysis, industrial gas manufacturing, and more. Due to its simplicity, nearly every SPR configuration uses a detection scheme consisting of a light source, sample, beam splitter or prism, and detector. This widely used configuration is called the Kretschmann configuration. In the current investigation we use a 532 nm laser which photons strike our silver nanorod array localized structure. This incident light strikes through the prism and interacts with the Ag's electrons. The photons are absorbed by the Ag's electrons, therefore

the electron field is influenced and surface plasma waves begin to oscillate on the surface of the Ag sample, represented in Figure 3.

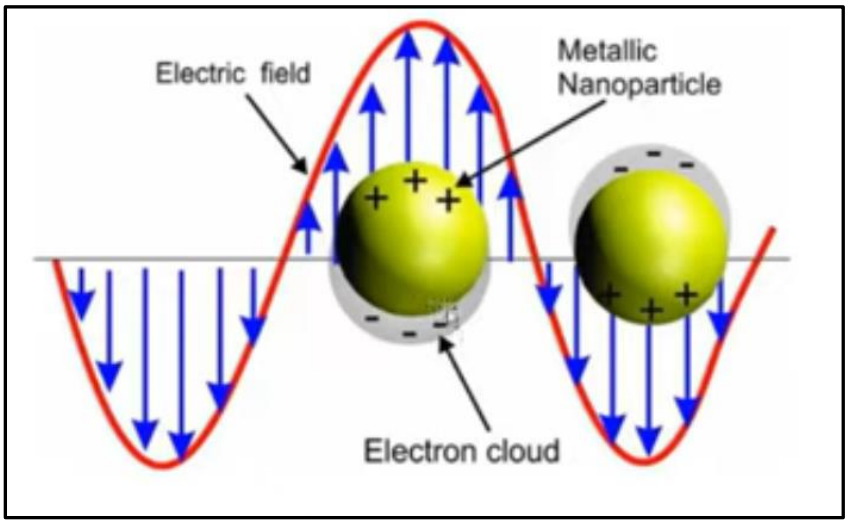

Figure 3: Example of the electrons surface plasmon wave when struck by incident light

Based on Mie theory, in conjunction with these relatively larger metallic nanoparticles, the signal spectra is significantly enhanced. (48) Ag is used due to its intrinsic ability to sustain SPR on the surface because of its specific absorption of light and sustained propagation of the wave through the solid. The signal is amplified due to the particle size, shape, and refractive index of our Ag nanorods. Furthermore, the oscillations are amplified when the shape of these particles is sharper such as our nanorods. An example of the interaction with Au nanorod's plasmon electron cloud and the coupled incident light creates the SPR as shown in Figure 4. [63]

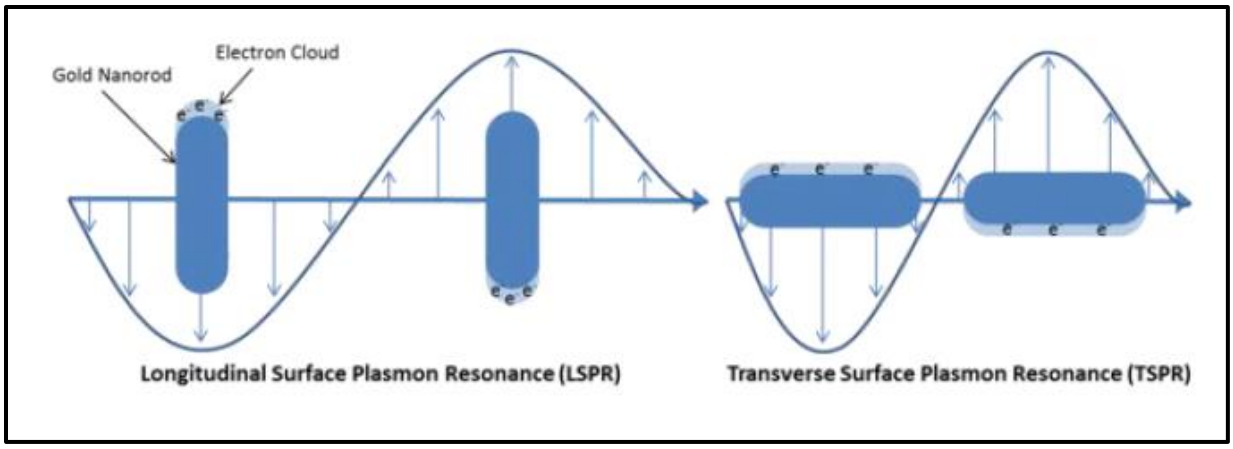

Figure 4: Example Au nanorods impact on SPR

The refractive index is another factor held accountable for enhanced SPR. In order for SPR to happen, the dielectric function real part is roughly negative two times the dielectric constant of surrounding medium. [64] When the incident light is directed towards the sample at the resonance angle, the photons of the light beam have a momentum equal to the momentum of the surface plasmons. This energy absorbed by plasmons causes a change of the reflection angle which yields the signal output of instrumentation such as Raman Spectrometers.

Raman Spectroscopy

Raman Spectroscopy is the analysis technique where a sample is exposed to a monochromatic, excitation laser that interacts with an analyte molecule. The sample absorbs most the light, but a small percentage is scattered in all directions where a CCD detector can acquire the data from position of sample the laser hits versus vibrational state as shown in Figure 5. [65]

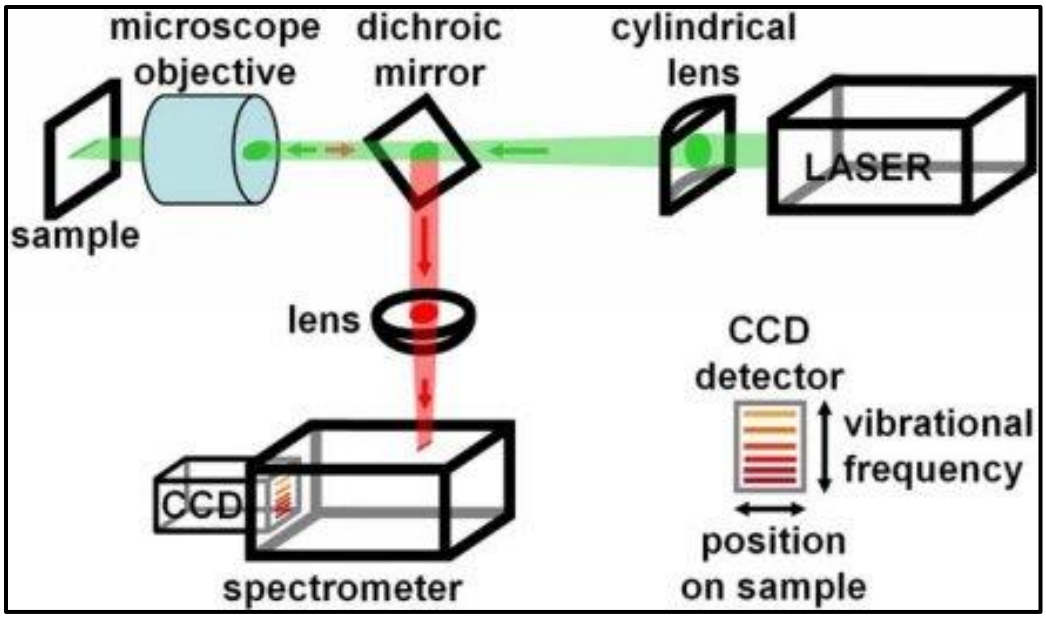

Figure 5: Example of the configuration used for Raman Spectroscopy

This incident light has an incident frequency. If the scattering frequency equals the incident frequency, (Vs=Vi) then this is called Rayleigh Scattering as shown in Figure 6. [49]

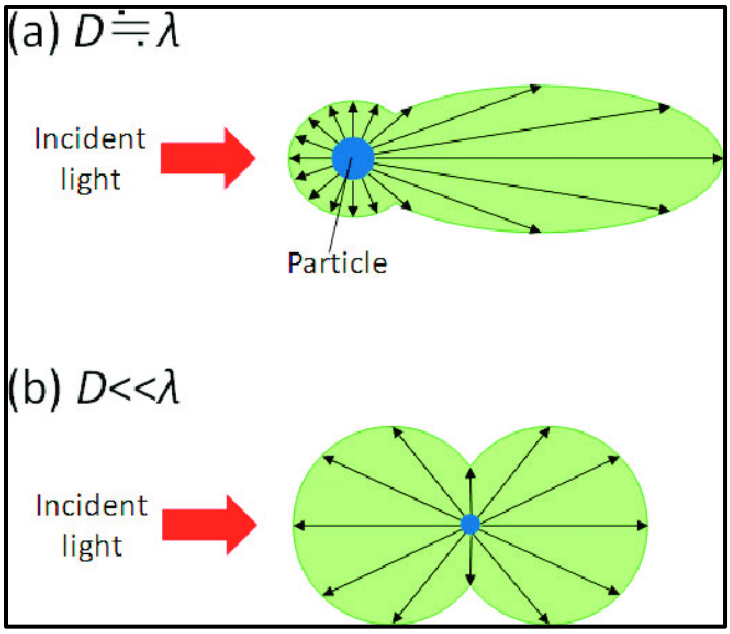

Figure 6: Figure 6a shows Mie scattering with the diameter of the particle approaching the same number as the incident light wave number. 6b shows Rayleigh scattering when the diameter of the particle is much smaller than the wave number.

Approximately 1 percent of the scattering intensity occurs at different frequencies than the incident frequency and this is labeled the Raman scattering. These electrons have different vibration levels defined as specific energy differences. The Raman Spectroscopy instrument will detect the Raman scattering and create a spectrum which can be analyzed to provide a structural fingerprint indicating specific molecules.

Furthermore, the electrons being hit by incident monochromatic light absorbs energy and rises to its Virtual Energy state (energy transferred = hVi) then the electron falls back to an energy level when losing energy. If the energy increased equals the energy lose then Rayleigh scattering occurs a photon emits. There are other times however, the energy is lost, and the electron falls back to a different vibrational level. Again, this is when the energy lost does not equal the energy that was absorbed from the incident photon. As a result, the photon emitted from the electron has a different energy than the incident photon. This gives rise to how the Raman scattering process occurs.

Depending on if the frequency of scattered photon is less than the frequency of the incident photon this will give stokes line or anti -stokes line, shown in Figure 7 [50], observed in the Raman spectrum.

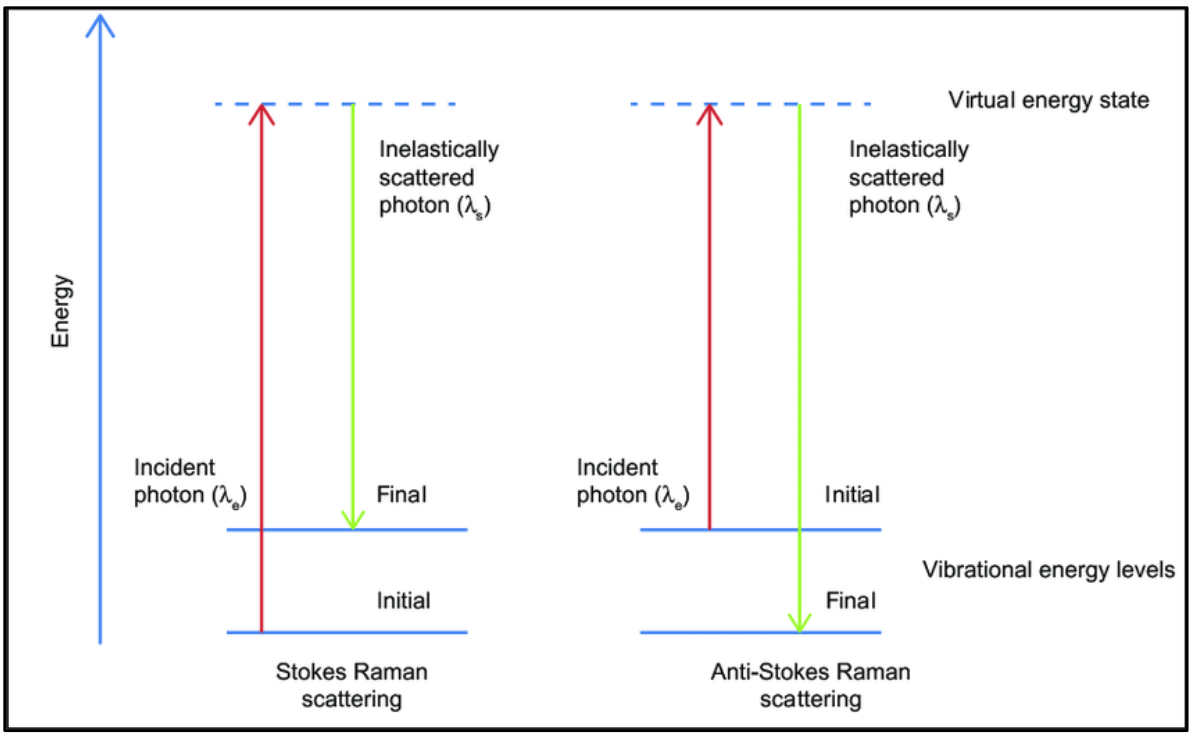

Figure 7: Raman scattering of (left) stokes scattering when vibrational energy levels shift up and (right) Anti-Stokes scattering when vibrational energy levels decrease.

If the frequency of scattered photon is greater than the frequency of the incident photon then Anti-Stokes lines are observed in the spectrum. The Raman spectra yields a molecular fingerprint. Different molecules have different Raman spectra. By studying the spectra, you can identify rotational levels and perform qualitative analyses. Additionally, you can study the spectra by looking at the particular Raman lines intensities to tell you about the concentration of a molecule in a sample, therefore giving you quantitative analysis.

Raman Spectroscopy is a widely established light scattering analysis used for many applications. Applications for Raman spectroscopy include Biomolecule sensing [24-27], single molecule detection [16-23, 27], detection of chemicals in water [15], Tumor Detection [14], and even NASA would like to try and detect signs of life on remote extraterrestrial locations using Raman spectroscopy. Raman has been underutilized for some time due to fluorescence

competition and due to the low amounts of Raman scattering from incident photons. Recently, Raman spectroscopy has gained notice in the nanoscience community with the evolved surface enhanced Raman spectroscopy (SERS). SERS has become available, with the addition of metallic nanostructures to the surface of substrates where the analyte resides. Normal Raman spectra, like the one shown in Figure 8 [66], relies on the inelastic scattering of an analyte molecule and sample matrix.

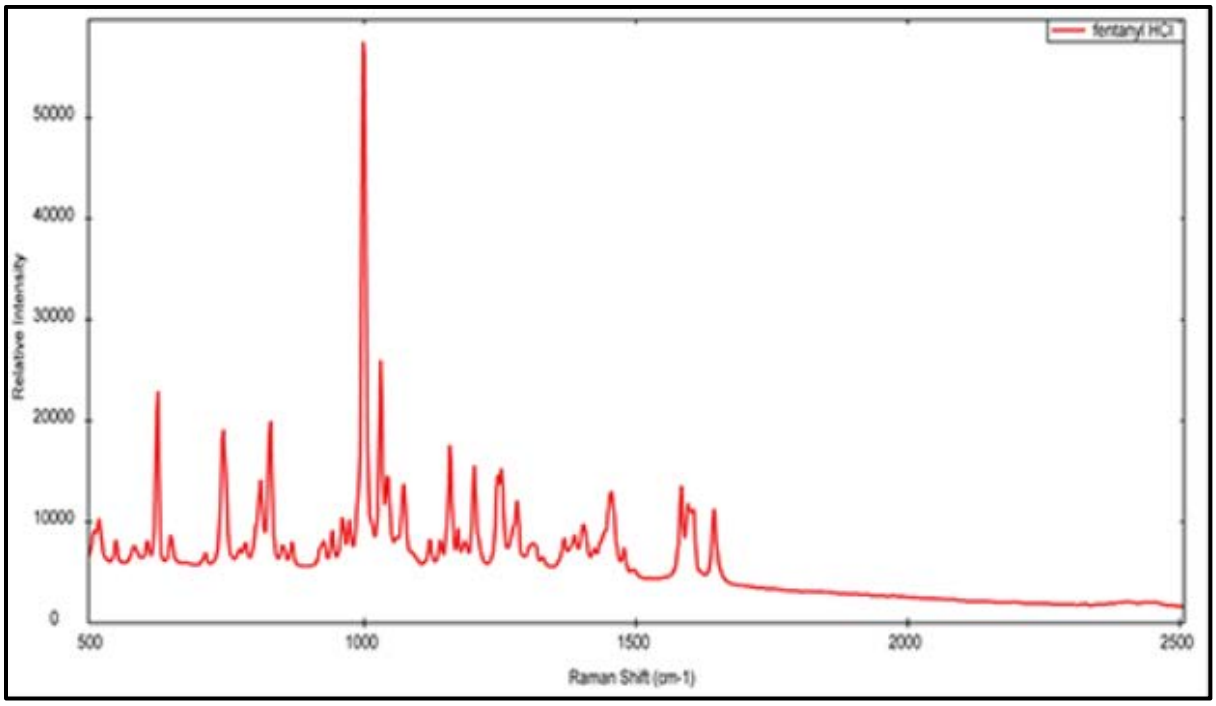

Figure 8: Normal Raman Spectra of Fantenyl HCI

Typical normal Raman samples need to be strongly scattering for detection limits to be approximately 1-10% concentration. [66] For applications involving virus detection these limits are orders of magnitudes to high. Some samples have small volumes where Raman Spectroscopy alone is inadequate for acquiring spectra. More recent application are involving samples with very low concentrations, or even traces. An evolved method was produced coined Surface Enhanced Raman Spectroscopy (SERS) to detect these small quantity samples. Unlike normal

Raman, SERS involves the vibrational modes of the molecule and the substrate the sample is absorbed upon, not solely the molecule. This attributes by the SERS substrate amplify the signal, in-turn opening another level for analysts to research low concentrations of samples.

Surfaced Enhanced Raman Spectroscopy (SERS)

Molecules with very low Raman efficiencies require improved Raman analysis such as SERS. The SERS effect is not completely understood and there are challenges that need to be discussed. Two mechanisms are believed responsible for the enhancement causes. The enhancement is believed to come mainly from a long-range electromagnetic effect due to optical properties of nanostructured metallic surfaces, a contribution 10^10. The second enhancement is caused from short range chemical effect due to charge transfer between the chemically absorbed species and the metal surfaces, a contribution of 10^2 [23]. These effects happen simultaneously.

The Enhancement effect depends on the geometry of the particle and substrate. Commonly used substrates are gold and silver nanoparticles. In the current research silver nanorod structures are used. Three aspects are considered when creating these SERS substrates. The following are considered; the nanoscale roughened surfaces onto which the sample is absorbed, colloid suspension of the sample, and the enhanced Raman signal depends on the shape and the size of the nanostructures. The Ag nanorods during the following experiments are approximately 100 nm diameter and 200 nm in length, grown by oblique angle deposition has been proven through significant literature to be ideal surface amplifiers for SERS [43, 67, 68]. This lead to Raman gaining traction in the interest for rapid detection of pathogens like COVID-19 strands which many recent reports are being produced. [69-71] In Chapter 4, Material Characterization section of this paper, we go into more of the spectroscopies used in this paper, but first an understanding of the substrate creation by physical vapor deposition is essential.

Chapter 3. Physical Vapor Deposition

Physical Vapor Deposition (PVD)

The nanofabrication community has three main choices in fabrication methods for nanomaterials: chemical vapor growth (CVD), physical vapor growth (PVD), and solution synthesis. For this investigation, neither solution synthesis nor chemical vapor synthesis will be used. CVD does not produce pure gold or silver nanorod surfaces because these reaction generally happen at higher temperatures. For solution synthesis the nanostructures are grown while free floating in solution, unlike the PVD which is grown on substrates. [53] Substrates make PVD better for Raman analysis. For solution synthesis or electrochemical methods, nanostructures are generally grown with capping agents to keep them from growing into bulk crystals. [54] An example of gold nanorods grown by solution synthesis is shown in Figure 9. [72] The surfaces of the capping agent will interact with the analyte you are trying to detect. PVD does not include chemical reactions. Instead PVD growth structure, includes sufficiently understood thermodynamics and surface kinetics in the bottom up evaporation-synthesis process. No capping agents are involved so the surfaces of the rods are ultra clean. The downside to PVD has been the spread in size and shape from self-assembly.

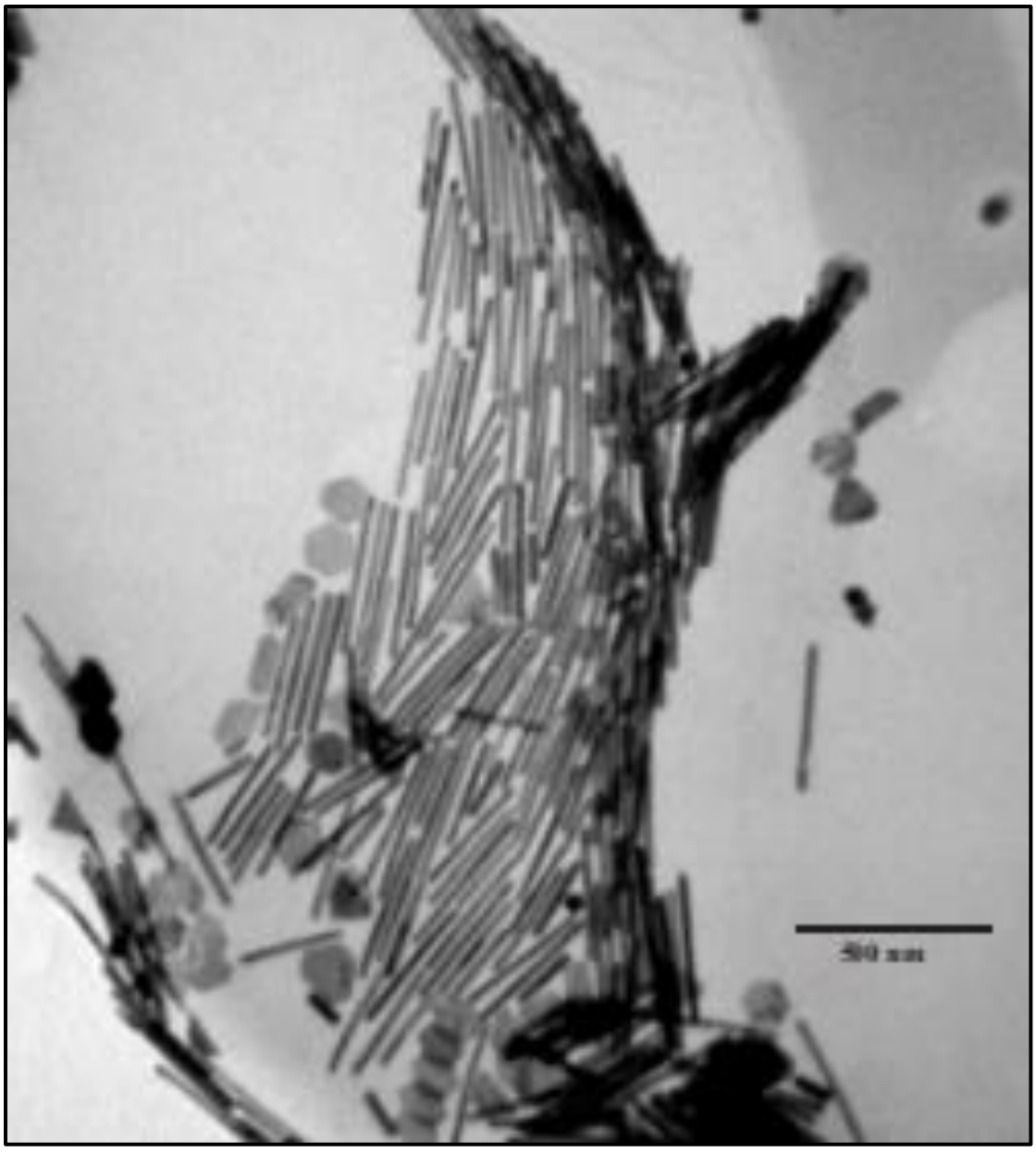

Figure 9: TEM image of gold Nanorod grown by solution synthesis. Aspect ratio of 25 and scale bar of 500 nm.

Two main PVD techniques are used to create nanostructures, sputtering and evaporation. Sputtering uses gas to generate a plasma to erode the source material shown in Figure 10. [51]

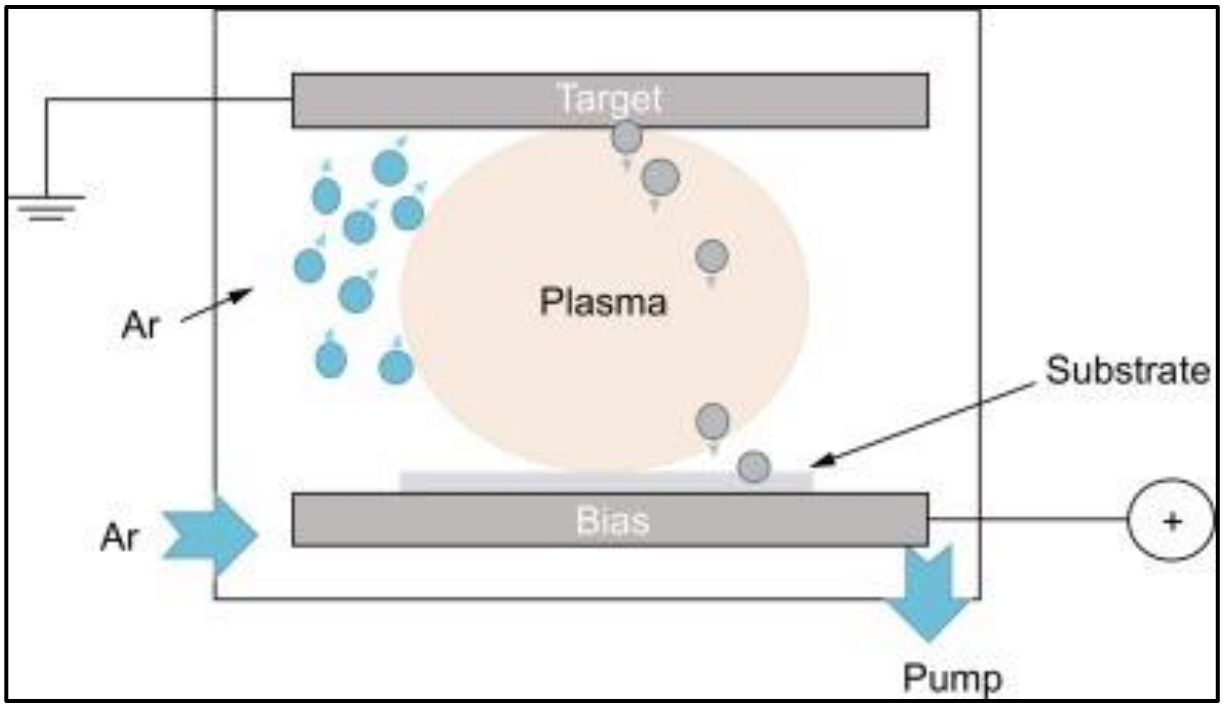

Figure 10: Configuration representation of Sputtering deposition by Argon gas.

This event creates gases that results in scattering and stops "line of sight" deposition onto a target substrate. [51, 52] PVD by evaporation to grow nanomaterials utilizes thermal, electron beam, ion bombardment, or laser ablation techniques sources. Of the PVD techniques, thermal evaporating is easy to implement, easy to scale, a low-cost system, and offers easily repeatable results. Thermal evaporating PVD consists of a vacuum chamber, where the source material is vaporized by resistive heating.

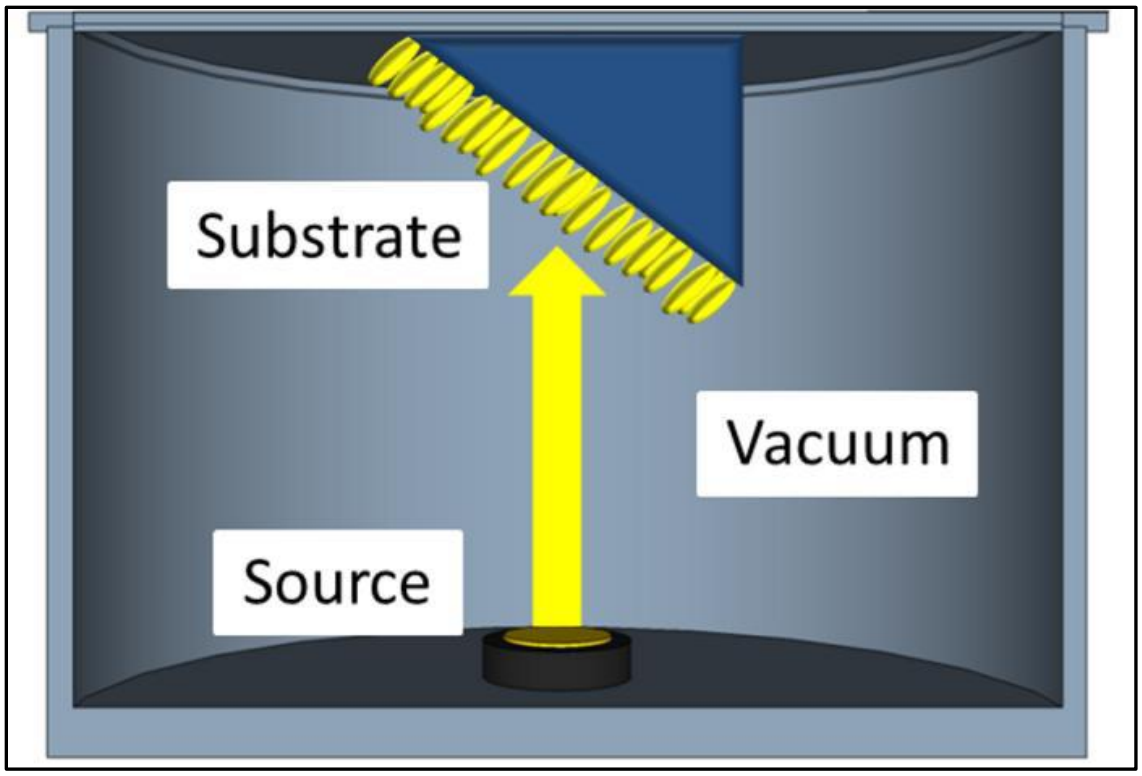

Figure 11: Physical Vapor Deposition Vacuum Chamber Representation. The source material is vaporized and travels through the chamber onto target substrate

The source material is put under sufficient heat such that the resistivity of the basket causes atoms to vaporize, shown in Figure 11 [13]. The source material can sublime, from solid to vapor, or in most cases, evaporates from liquid to vapor after melting from solid to liquid. The process relies on when materials are heated, there is a finite vapor pressure over all materials. Before the source material can be deposited onto the sample, evacuation of the chamber gases is required.

The PVD chamber typically has an inert gas inlet and outlet pumps to create the vacuum. The pumps consist of a rough and turbo pump, shown in Figure 12. The rough pump will create a suction to rid of most the gases. Once the gases go below viscous flow the turbo pump will suction and evacuate the chamber gases to reduce pressure to approximately 10^-2, which is required before vaporizing any source material. In these low pressures, is what creates idea flow

for molecules without scatter. The ideal flow for molecules is called the mean free path, where the source material has a direct line of sight and the vacuum will cause deposition in a straight shot onto the target sample. After achieving the low pressure in the chamber, then can the experiment begin proceeding with resistive heating of the sample.

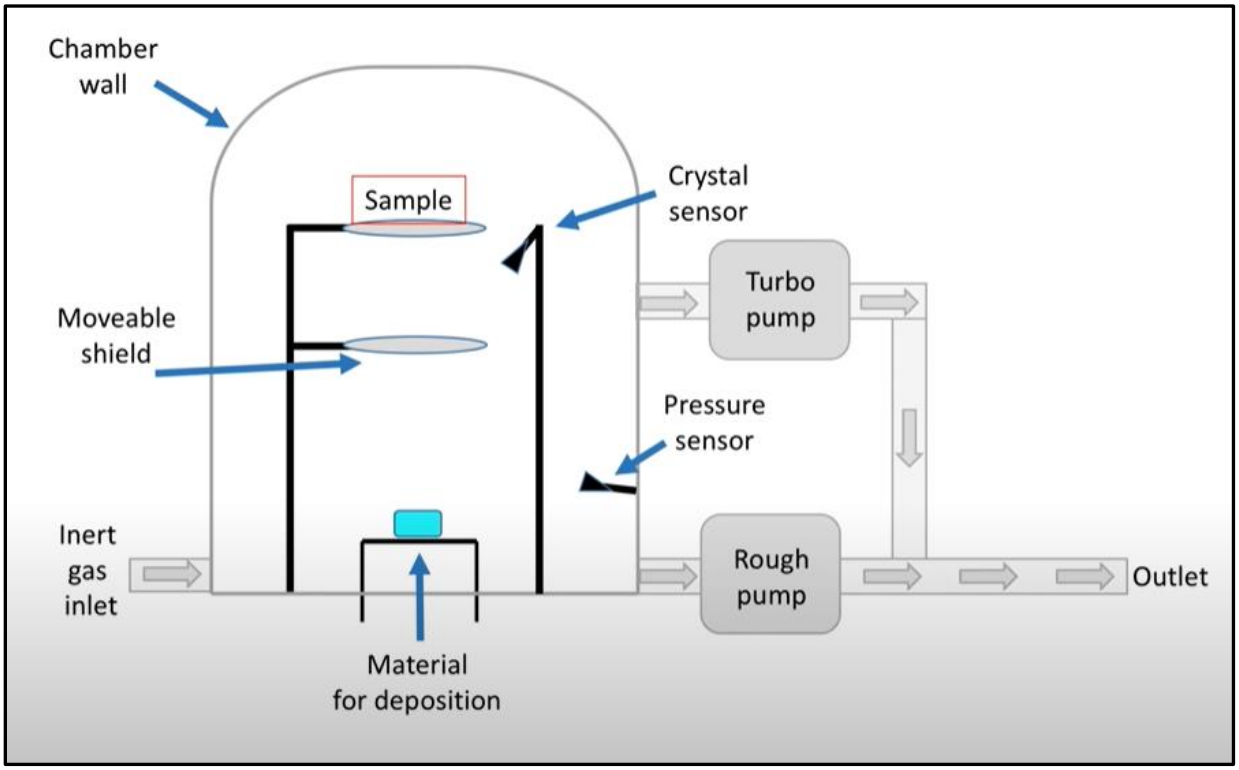

Figure 12: Representation of a PVD configuration with a quartz sensor for deposition rate

Thermal energy is supplied by passing a large current through a thermally tolerant basket, for example tungsten, which is holding the source material. These vaporized atoms travel through a low-pressure space where the flux of atoms rise until they hit the downward facing target sample, where the atoms condense and forms a film sample. A quartz crystal sensor enables control of source material vaporization rate, shown in Figure 12. This quartz microbalance uses vibrational frequency to detect rate. The microbalance contains a crystal perpendicular to the flux and when mass is added by deposition the vibration frequency will change as well. This rate control can be

coupled with a movable shield to allow specific film thickness deposition on the target sample. Due to the pure nature of these metal films, many applications for coating have stemmed from this method [4-12]. Besides coating materials, PVD is used in the application of growing nanorods to create surface enhanced Raman spectroscopy (SERS).

Oblique Angle Deposition

Over the last century there has been sufficient progress in the nanofabrication technology of PVD, two advanced methods, GLAD [2,3] and OAD [1] in particular, have shown significant promise for growing nanorods. For the current experiments PVD is the fabrication method where synthesis of silver (Ag) nanorods occur on an oblique angle glass slide by evaporation in a vacuum.

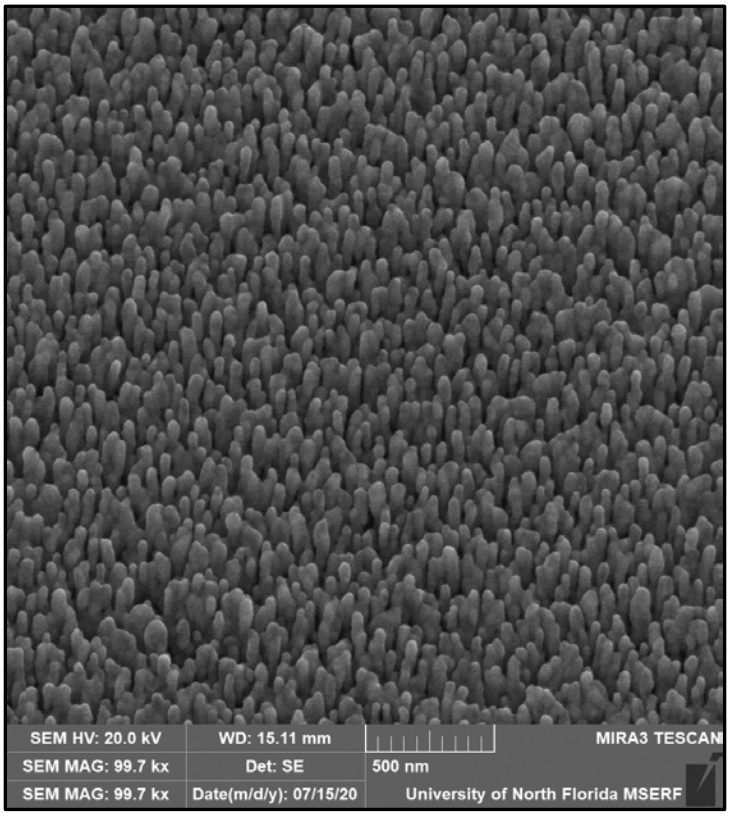

Figure 13: Representation of Ag nanorods from an TESCAN SEM

These syntheses of Ag on the glass slide are nanorods growing at approximately the 100 nm range dimensions shown in Figure 13. This angle introduces a geometric shadowing effect where the Ag nanorods can grow uniformly. Geometric shadowing happens when adatoms diffuse to the target surface at low temperature and such a high deposition rates that adatoms start to grow on top of each other creating islands. Once islands start to form, due to shadowing of these islands, adatoms only start to land on top of adatoms until you for rod growth only, shown in Figure 14.

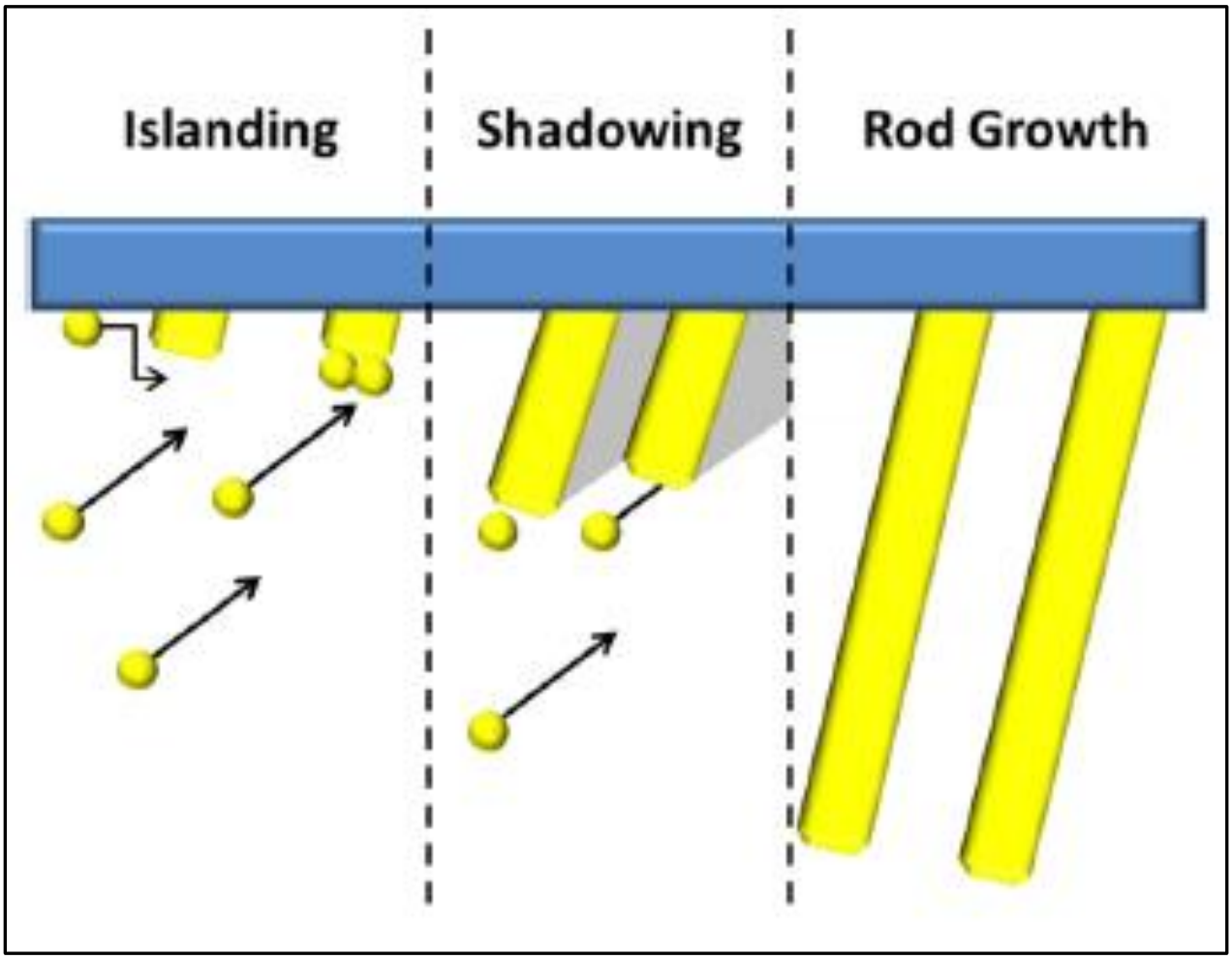

Figure 14: Geometric shadowing process of nanorod growth

Thermodynamics in PVD Growth Nanorod Structures

An easy example to help visualize this scale of nanorods is to picture hair on a single strand of human hair. This is the scale this nanoscience community works in, which tends to be under 100 nanometers. To understand the thermodynamics in nanostructure crystal growth from PVD, starting with the fundamentals of crystal growth in general will yield better results in grasping this concept. Crystals grow in continuous shapes mostly due to their atoms organized, repeating patterns. Crystalline structural growth depends on how the atomic pattern is arranged. If the atoms pattern arrangement is cubic, then the crystal tends to grow in a cube shape. Another example of cubic lattice is Silver, with a face centered cubic (FCC). FCC structures have atoms covering 74 percent volume in their lattice, which makes up for the highest close packed of all crystal lattice structures.

In any case, a phase change has to occur that is thermodynamically desirable. In this case, phase change is born from a solution or vapor. The source material vaporizes and travels across the vacuum chamber onto the target sample. Here the adatom can integrate into a crimp or irregularity in the surface or nucleate a new layer.

In order for the nanostructures to grow into rod-like structures the chamber of PVD must be in a non-equilibrium state. PVD is always in a state of supersaturation. Furthermore, the adatoms final location depends on diffusion barriers and thermal energy. If an adatom has insufficient energy, the likelihood of mobility is decreased. [13, 73] Based off the Kossel model, it is three time more likely for an adatom to step or diffuse to another monolayer instead of making a multi-layer jump. Therefore, once the nanorods is formed, the probability of growth is high. [13,73,74] If the deposition rate during PVD is high, the adatom that hits the target surface can be hit by another adatom before it diffuses. Two adatoms form a dimer, which creates a

much higher diffusion barrier to overcome. [13] The mobility of a dimer is therefore restricted. High deposition rate gives rise to surface roughness through an abundance of 3D morphing and nanorods. [13]

A second means of increasing surface roughness is to lower the temperature in the vacuum. By lowering the temperature in the vacuum, this lowers the thermal mobility of adatoms which in turn the diffusion barrier kinetically dampens the adatom from movement. [13,73] Again, this results in higher introduction of 3-dimensional growth of nanorod structures.

Silver as the Source Material for Nanorods Growth

In PVD, three main challenges exist in the fabrication of silver nanorods. In this work we will discuss (1) how does surface diffusion participate in the formation of Ag nanorods and the diameters of these nanorods? We will need to look into the deposition rate and temperature, as the surface diffusion relies on these factors. We would like to create nanorods with the smallest diameter possible, therefore a closed form theory will be indicative in how these two factors associate with one another. (2) At the same time, it is necessary to understand the nanofabrication of such nanorods to create a sufficient spacing between nanorods. If the columns are grown too close to each other they will coalesce, where separate columns will not grow. Further, we will need to control the spread of nanorods to not having a big distance from each other, so the adatom do not start to form on the side of the columns which would increase the diameter of the rods. (3) We will need to find a way that silver does not corrode in harsh environment for SERS.

The Corrosion of Silver

All metals can corrode. In the nanoscale realm, with decreased surface area and harsh environments, corrosion contamination can happen in minutes even with noble metals like silver. Corrosion in metals happen by electrochemical reactions when the metal comes in contact with its surrounding environment specifically atmospheric gases. Based on the environment, this will depend on the corrosion form and rate of deterioration. For SERS samples, the corrosion of silver presents a problem in itself. When Ag nanostructures is exposed to harsh environments, which can be as simple as storing in air, hydrogen sulfide can corrode the Ag substrate. In less than a day of Ag exposed in these environments, AgS will begin to form a black coating on the outside surface. [40] These corroding contaminates of Ag can diminish results for Raman spectra.

Similarly, discussed previously, Ag nanostructures stored in liquids, even distilled water, will corrode in a matter of minutes after the AgO forms. [43] A method will be discussed in the latter sections of this work to eliminate corroding for relatively long periods of time of silver by preventing contact of the harmful atoms. One of the more advanced methods in PVD for creating these Ag nanorods is used for the current experiment by Oblique Angle Deposition (OAD). These OAD nanorods are part of the prevention procedure discussed later.

Many research efforts and large sums of funding have been conducted in the past decades to strive to improve technology or invent technology by studying nanomaterial in the 100 nm range. More recently, nanomaterials in the 10 nm range have been of interest. The nanomaterials in the 10 nm range is the focus due to the potential to impact nanotechnologies that are relevant in current societal problems. One of today's societal problems include understanding the SERS phenomena and why it enhances signals by 10^11. Enhancing Raman signal can be induced by

creating metallic nanorods for SERS substrates. OAD is a method to fabricate Ag nanorods for SERS samples.

Chapter 4. Materials Characterization

Scanning Electron Microscopy (SEM)

SEM works with a configuration of an electron gun that supplies a voltage through a tungsten filament onto a thermionic cathode which shoots an electron beam into a vacuum chamber. This beam accelerates through an anode, a set of condenser lenses, and an objective lens in a vacuum chamber which guides the electrons by electromagnetic fields into the sample chamber as shown in Figure 15. [75]

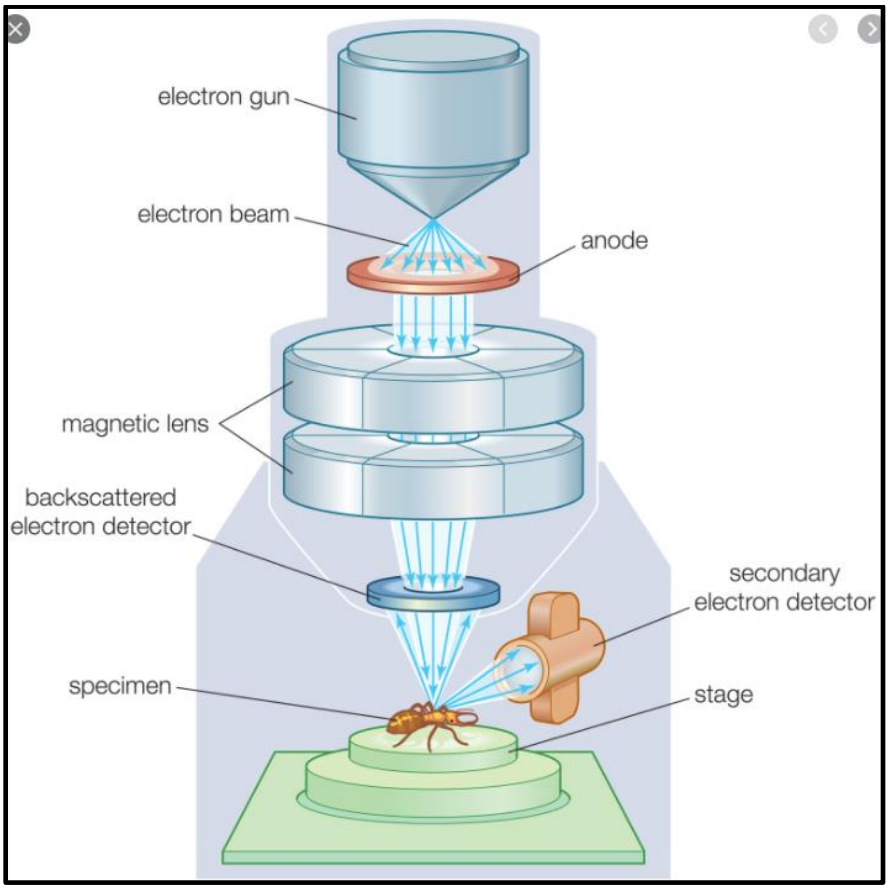

Figure 15: The image is a representation of the configuration for a Scanning Electron Microscope (SEM).

The beam then strikes the sample, on the positively charged sample stage again guiding the negatively charged beam of electrons, and data is collected through the EDS X-ray detector, backscatter detector, and secondary detector. When the beam strikes the sample emits secondary electrons off the surface which yield desired surface images created by the secondary detector. The beam then penetrates deeper where the sample emits off the surface and within the sample back scatter electrons which is how the backscatter detector creates images. At the same time, some of the back scatter electrons get trapped in the sample which is where x-rays are emitted and can be captured for elemental analysis by an energy dispersive spectroscopy (EDS) detector as shown in Figure 16. [76]

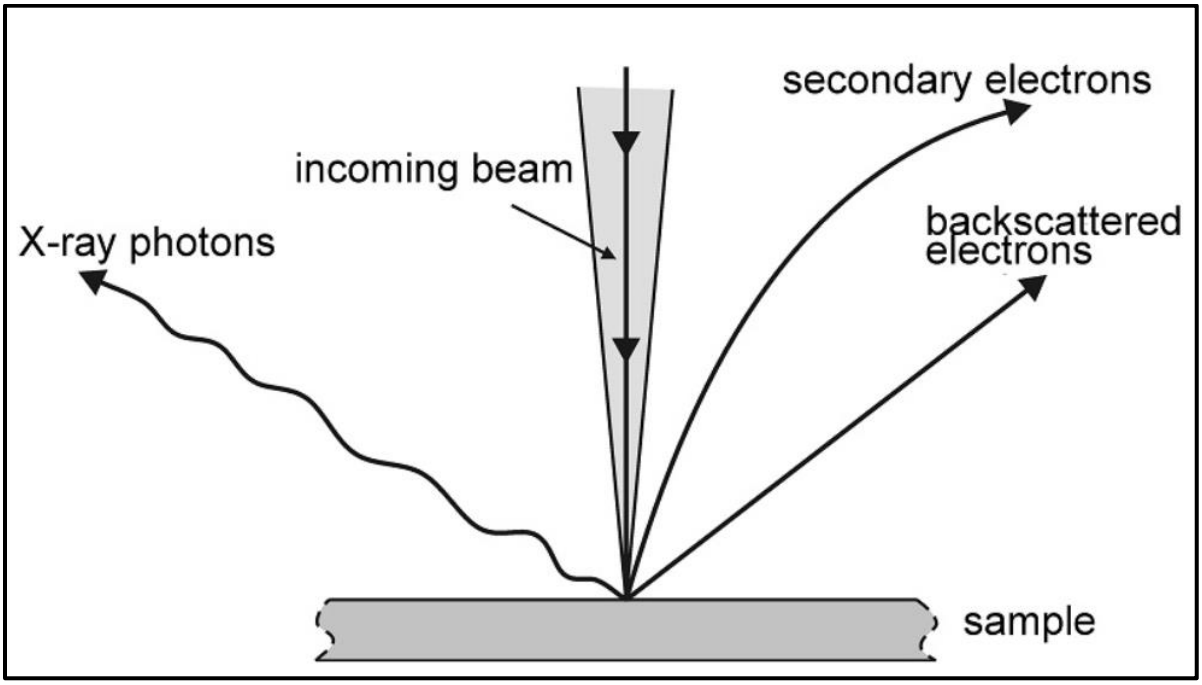

Figure 16: The image is a representation of the sample-electron interaction from the incoming electron beam.

Scanning Probe Microscopy (SPM)

SPM is a surface analysis technique with various modes to characterize mechanical properties such as electrochemical reaction, adhesion force, young's modulus, and several other

properties. Two modes of particular interest are the contact mode for surface topography and Kinetic Force Probe Microscopy (KFM) for surface potential. The contact mode runs a nanometer size probe that physically comes in contact with a sample raster scanning a localized area of a sample as shown in Figure 17. [47]

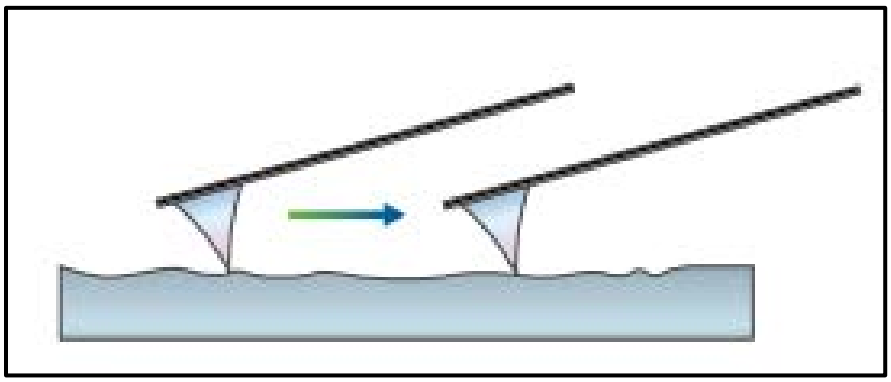

Figure 17: The cantilever tip traces and retraces a localized section of the sample in contact mode to obtain topographical images.

The contact mode creates an image by the SPM's laser detecting deflections of the cantilever which is discussed in the latter of this section. Contact mode is later discussed in the experimental section of this paper to show the surface topographical differences between the sample out of vacuum versus the sample that has perished in non-degassed water for 2 hours.

KFM mode yields the electric potential in voltage (V). During KFM the SPM supplies a small current for the conductive tip which when scanning the sample can analyze the difference in potential between the probe and the sample. A representative image between the cantilever and sample during KFM mode is shown in Figure 18 [47] for ease of visualization.

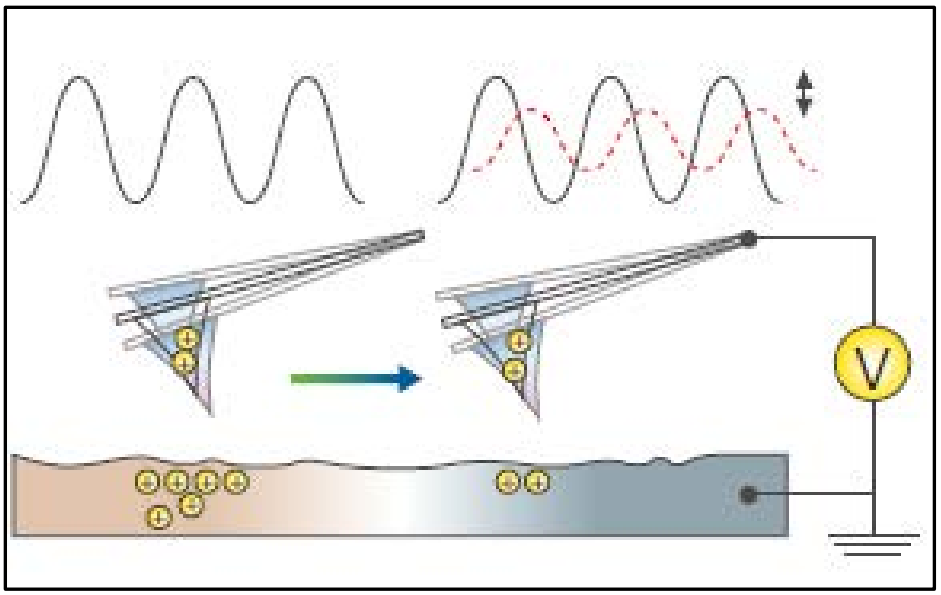

Figure 18: The image is to represent the interaction of the SPM cantilever conductive tip and the sample surface to obtain electric potential of a sample.

KFM mode is of interest to see how the surface potential of the sample material changes with a vacuum sample versus an oxide sample.

The SPM head contains the cantilever holder, the sample stage, laser, detector, and scanner shown in Figure 19. [47]

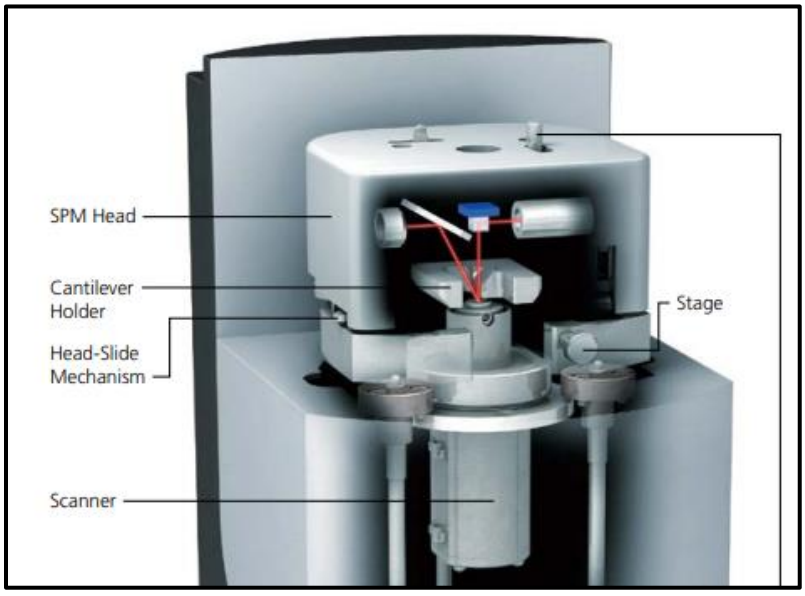

Figure 19: The SPM head and internal components.

The laser is how the SPM acquires topographical images. The laser beam is split with a beam splitter that directs the beam onto the top of the cantilever which then bounces onto another mirror which finally hits the position sensitive detector. The Piezoelectric scanner raster scans the sample stage in the X, Y, and Z axes to keep a desired interaction with the cantilevers probe shown in Figure 20. [77] This allows the probe to trace and retrace a localized sample section relatively quickly using contact or KFM modes.

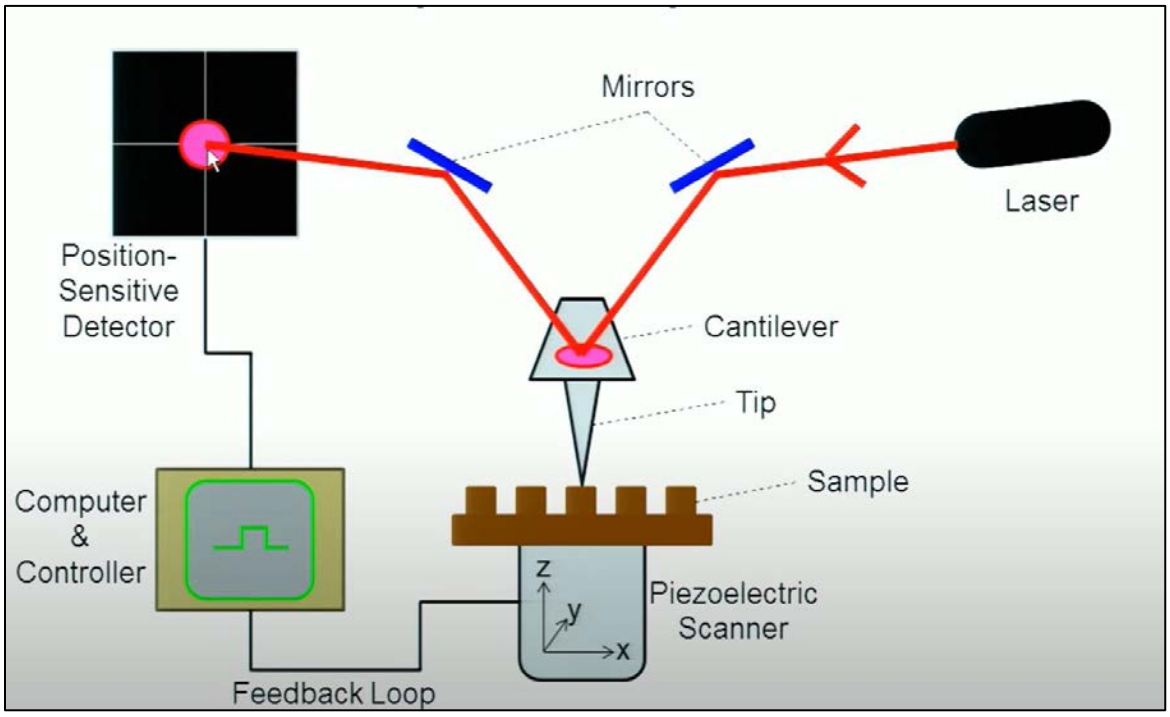

Figure 20: The typical internal components inside an SPM head.

Chapter 4. Experiment Methods

After nearly 30 years of laboratory scale research, metallic nanostructures are finally poised to propel existing and new technologies to meet critical needs in society [28-31]. One such current need is the sensitive, rapid, and low-cost detection of the SARS-CoV-2 virus, which is responsible for the devastating Covid-19 illness [32-33]. Classical detection techniques rely on the replication

of the viral RNA and are expensive and slow [34]. In the literature, sensors that rely on the unique optical properties of metallic nanostructures have been widely demonstrated to be rapid and potentially inexpensive at scale [35-38]. These optical sensors typically rely on the plasmonic properties of noble metal nanostructures, like silver nanorods or nanoparticles. The plasmonic properties of these nanostructures derive from a combination of length-scales less than 100nm and appropriate electronic work functions [39]. The functionality of these nanostructures as sensors relies heavily on the surfaces of the metallic nanostructures and binding or proximity of the targeted material to the surfaces [40]. The changes that happen within minutes to the surfaces in the presence of the targeted material are measured using optical ultra-violet visible spectroscopy (UV-Vis) or Raman spectroscopy [41].

Unlike in ideal laboratory conditions, the conditions experienced by these nanostructures in sensing applications are diverse and not well studied. In biological sensing applications, many different materials, like phosphate buffered saline, are required to maintain appropriate biological conditions [42]. The effects of these new materials on the morphological and chemical structures of metallic nanostructures has not been the topic of sufficient investigation in the literature. As such, observed differences and claims of detection of biological materials, like SARS-CoV-2, may be observations of changes to the metallic nanostructures caused by buffers and additives rather than the target molecule itself. For example, an extensive review of the literature shows that there has been no investigation into the effects of something as simple as the presence of dissolved gases in the water used in sensing experiments with metallic nanostructures like silver nanorods. However, it is well known in the literature and industry that dissolved oxygen in water can rapidly corrode silver [43].

In this technical document, a representative study, the authors demonstrate that significant differences exist in the optical reflection and Raman signals of rhodamine-6G (R6G) absorbed onto the surfaces of silver nanorods when the samples were exposed to di-ionized water versus the same water that had been degassed via boiling. Through investigation using scanning electron microscopy (SEM), post operation and in-situ UV-Vis spectroscopy, scanning probe microscopy (SPM), and Raman spectroscopy the authors determine that significant chemical and morphological changes occur when silver nanorods are exposed to water that has not been degassed, compared to negligible measured changes when they have been exposed to appropriately degassed water.

Prior to presenting the results we will briefly describe the experiments performed in this investigation. The experiments involve the fabrication of Ag nanorods using glancing angle physical vapor deposition (GLAD PVD), preparation of components and materials used in the study, and then the characterizations carried out using SEM, SPM, UV-Vis spectroscopy, and Raman spectroscopy.

Nanorod fabrication

Silver nanorods are grown using a PVD technique called glancing angle deposition. These nanorods were created in a custom-built high vacuum chamber by thermal evaporation [40,45,46] shown in Figure 21.

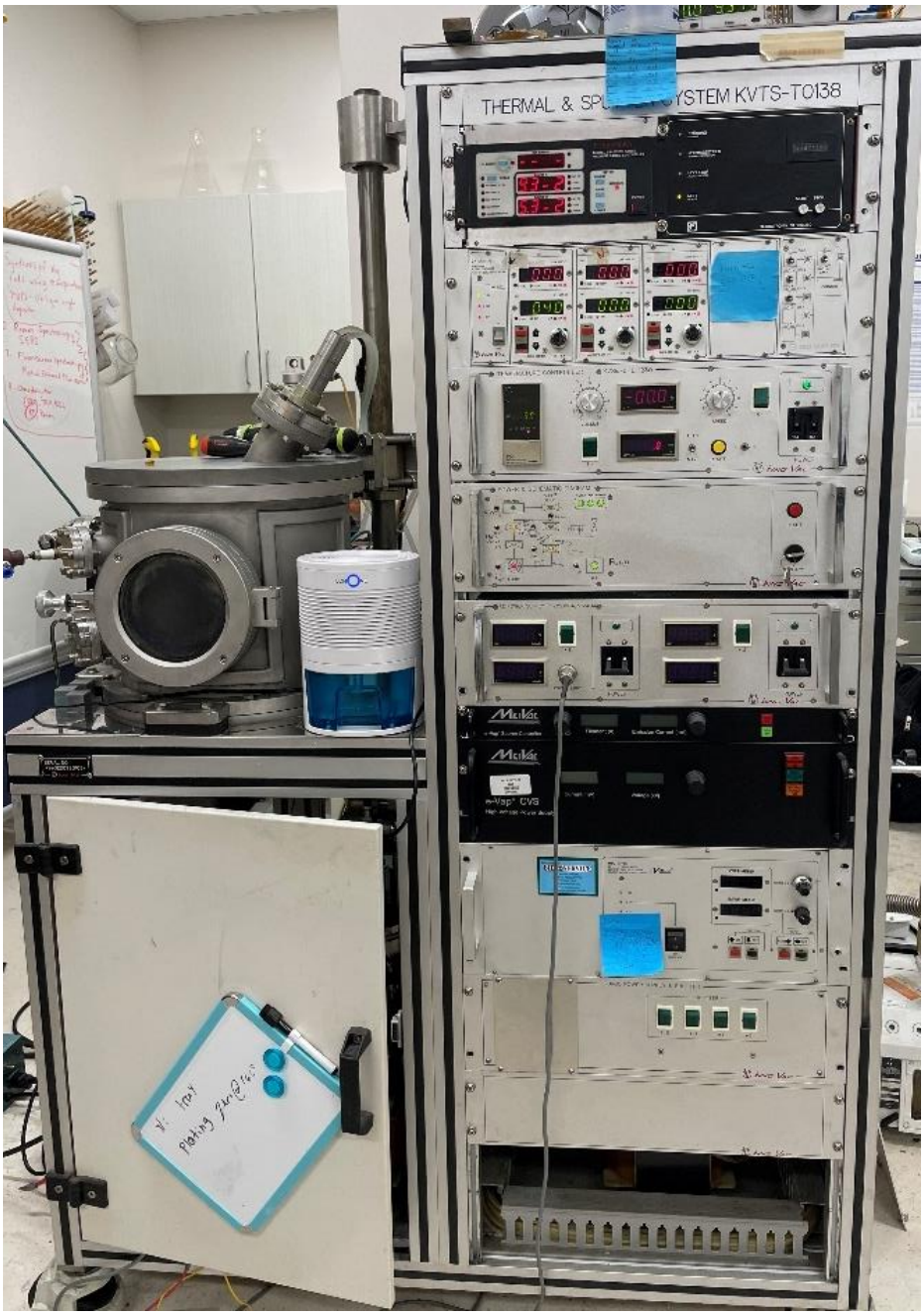

Figure 21: PVD System configuration with the custom-built high vacuum chamber on the top left

The vacuum chamber is a stainless-steel cylinder with a diameter of 30cm and a height of 20cm shown in Figure 22.

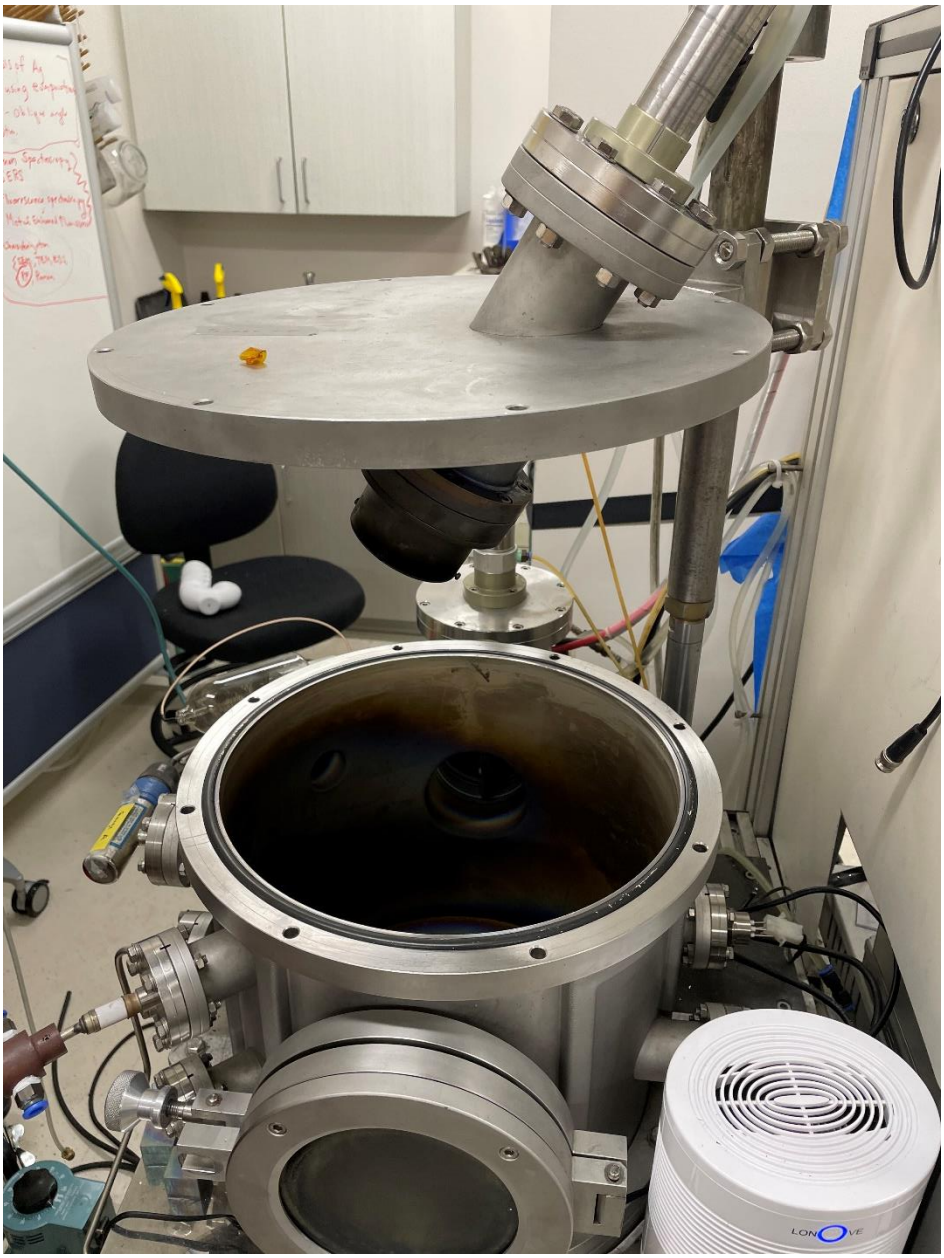

Figure 22: Close up of the Vacuum chamber

First, corning glass slides the Ag nanorods are grown on need to go through a thorough cleaning process. The slides are cleaned sequentially by sonication in acetone, ethanol, and di-ionized water for five minutes at each stage. The cleaned slides are then dried under a gentle flow of high

purity nitrogen. The slides are then mounted on a substrate holder at the top of the vacuum chamber after drying shown in Figure 23.

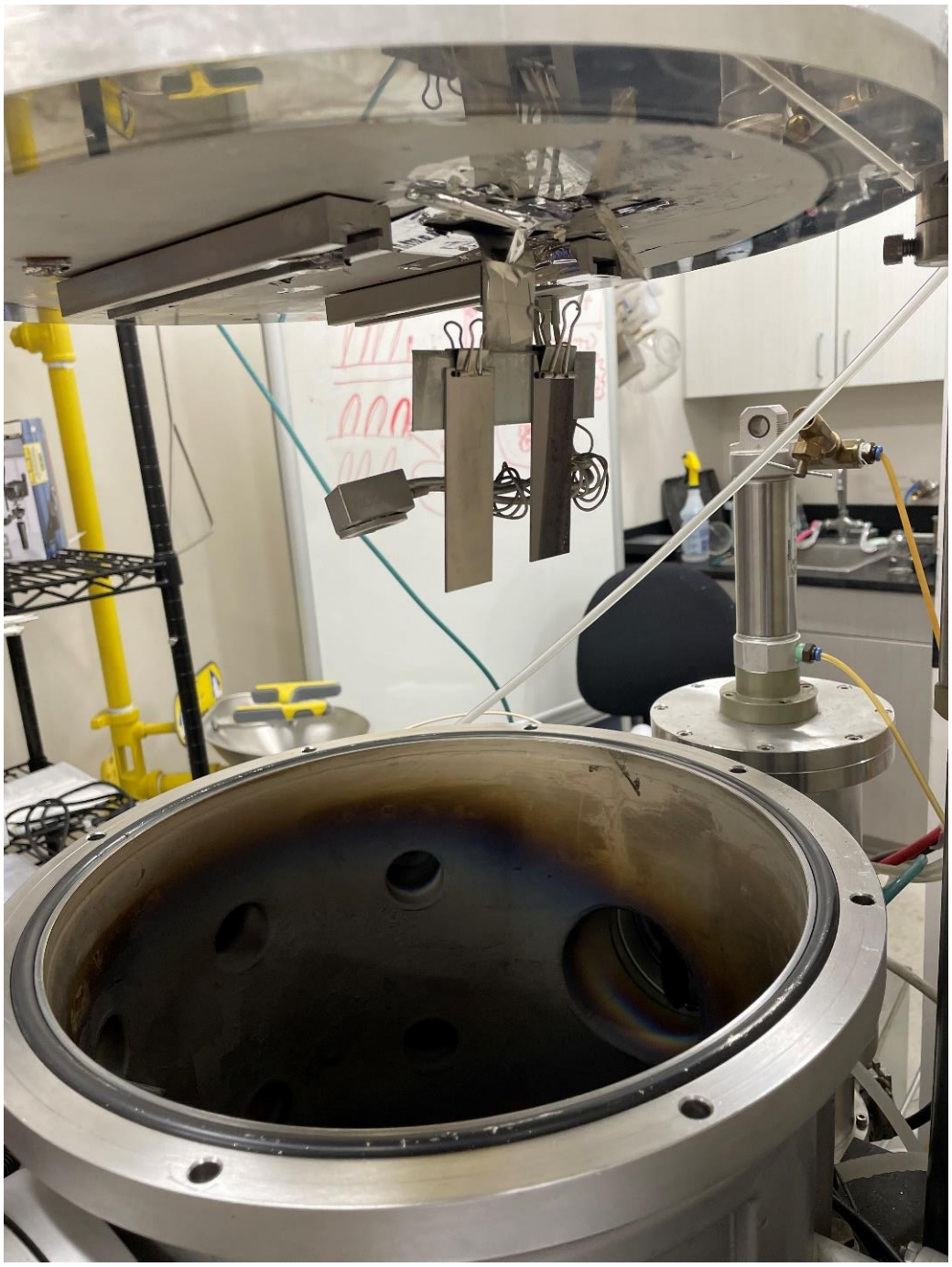

Figure 23: The corning glass fixture after Ag nanorods have been grown.

The thermal evaporation source is about 25 cm from the slides, at the bottom of the chamber. To achieve a glancing angle condition, the slides are angled at an incident angle of 87° relative to the source normal. To extract excess adsorbed water from the container, a mechanical roughing pump and a turbomolecular pump are used to evacuate the chamber until a vacuum of 5 x 10-5 Torr is achieved and sustained for an hour. Evaporation is carried out using 99.99 percent Ag pellets from a tungsten boat (Kurt J. Lesker Co.). The deposition rate is regulated to 10 A/s +/- 2 A/s for a total film thickness of 500 nm using a quartz crystal microbalance. After that, the samples are held under low to medium vacuum and only extracted before the next experiment.

Degassing of Water

A Millipore device produces high-purity deionized water, half of which is degassed by boiling. To degas, the water is put in a vacuum-sealed glass, Mason Jar-like, container, removed during boiling, and heated to rapid boiling on a laboratory hot plate. The water is brought to a boil for 15 minutes before being sealed with the vacuum tight lid. The sealed jar is then allowed to cool to room temperature naturally. It has been shown with the Dissolved Oxygen Meter the DI tap contains about 6 ppm of dissolved oxygen while this boiling process can provide water with as little as 1 ppm of dissolved oxygen [44].

Scanning Electron Microscopy

A Tescan Mira scanning electron microscope with an Oxford energy dispersive spectroscopy system is used for SEM (EDS) shown in Figure 24.

Figure 24: Tescan Mira3 SEM used to obtain sample images and EDS spectrum

Secondary electrons and x-ray photons are detected at magnifications up to 100k X with beam voltages of 10kV and working lengths of 10mm to model samples. Ag nanorod samples are imaged directly after being removed from vacuum and after being exposed to degassed and non-degassed water, followed by drying in a gentle nitrogen flow.

Scanning Probe Microscopy

The Shimadzu SPM-9700 HT is used for SPM. A 10 micron scanner attachment, fiber optic light source, and a high magnification CCD optical microscope unit are included in the SPM configuration shown in Figure 25.

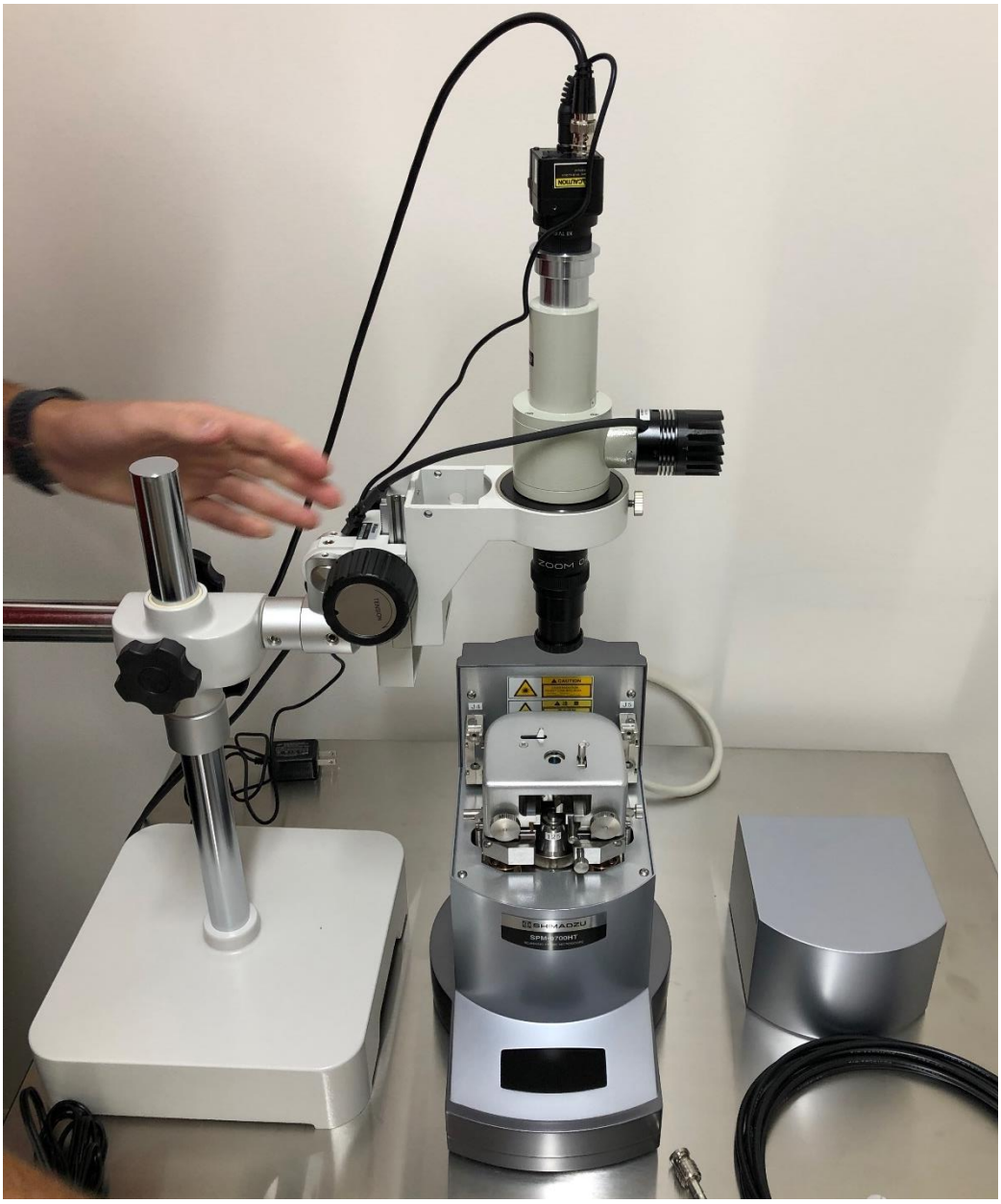

Figure 25: Shimadzu's SPM 9700-HT used for topographical observations and KFM analysis. SPM was carried out on specimens grown on 12.7 x 12.7 mm corning glass substrates with evaporated silver nanorod films as shown in Figure 26.

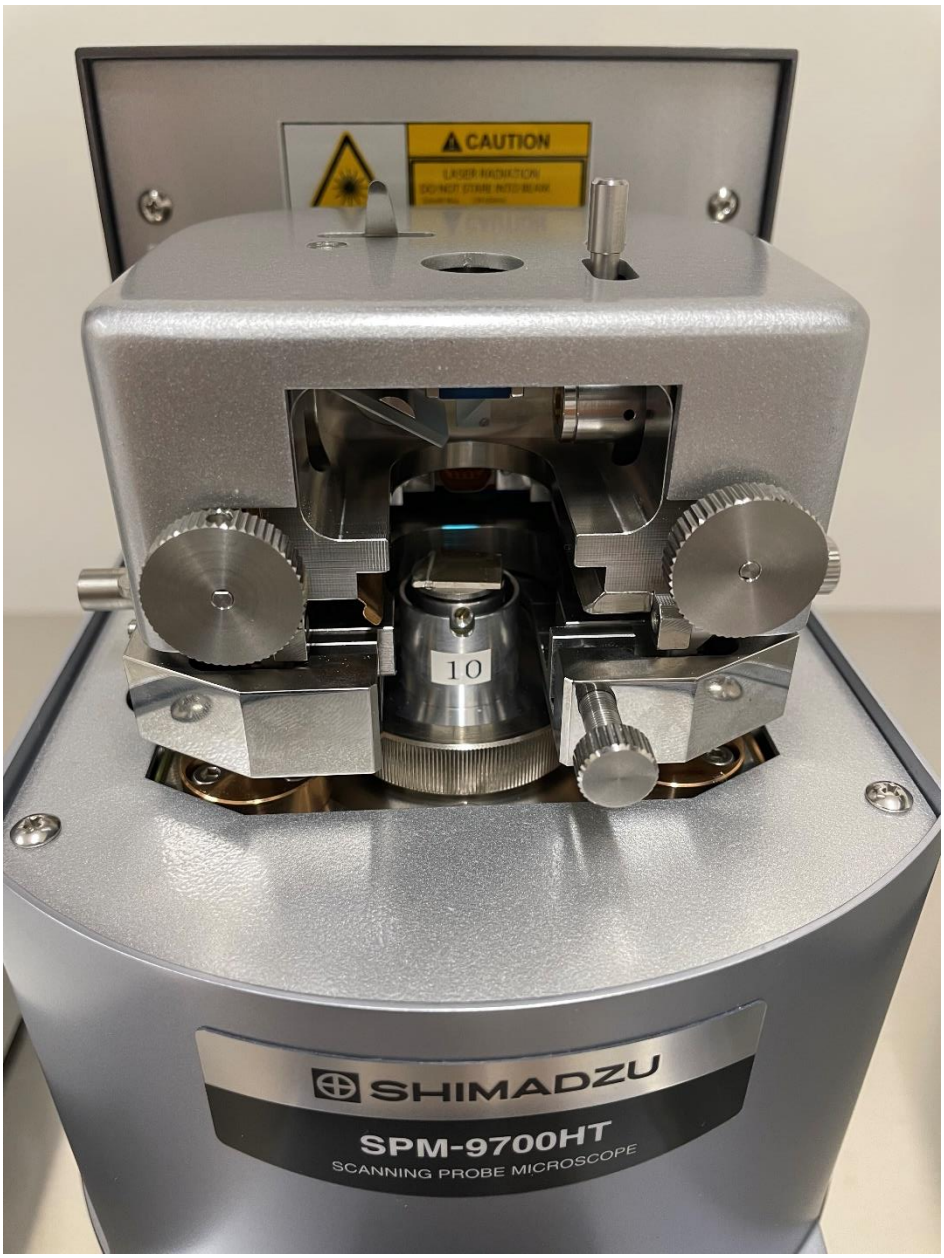

Figure 26: Ag glass sample sitting on the 10 micron scanner.

The raster scanning frequency was set to 1.00 Hz, and the pixel size was set to 256 x 256. The samples were first taken out of vacuum and imaged right away. The samples were then exposed to non-degassed water for two hours before being dried under a gentle flow of dry nitrogen and observed. The sample surfaces' topographical maps were created using contact mode. Second, the SPM was used in Kelvin Probe Force Microscopy (KFM) mode to examine surface potentials

and detect chemical changes on the surface. KFM is a noncontact variant of SPM in which the probe is placed at a constant height above the sample and a voltage bias is applied, allowing the surface to be mapped locally. Kinetic Probe Force Microscopy provides information on the specimen material's local electric surface potential.

UV-Vis

A Shimadzu UV-3600 with an integrating sphere attachment is used for UV-Vis spectroscopy as shown in Figure 27.

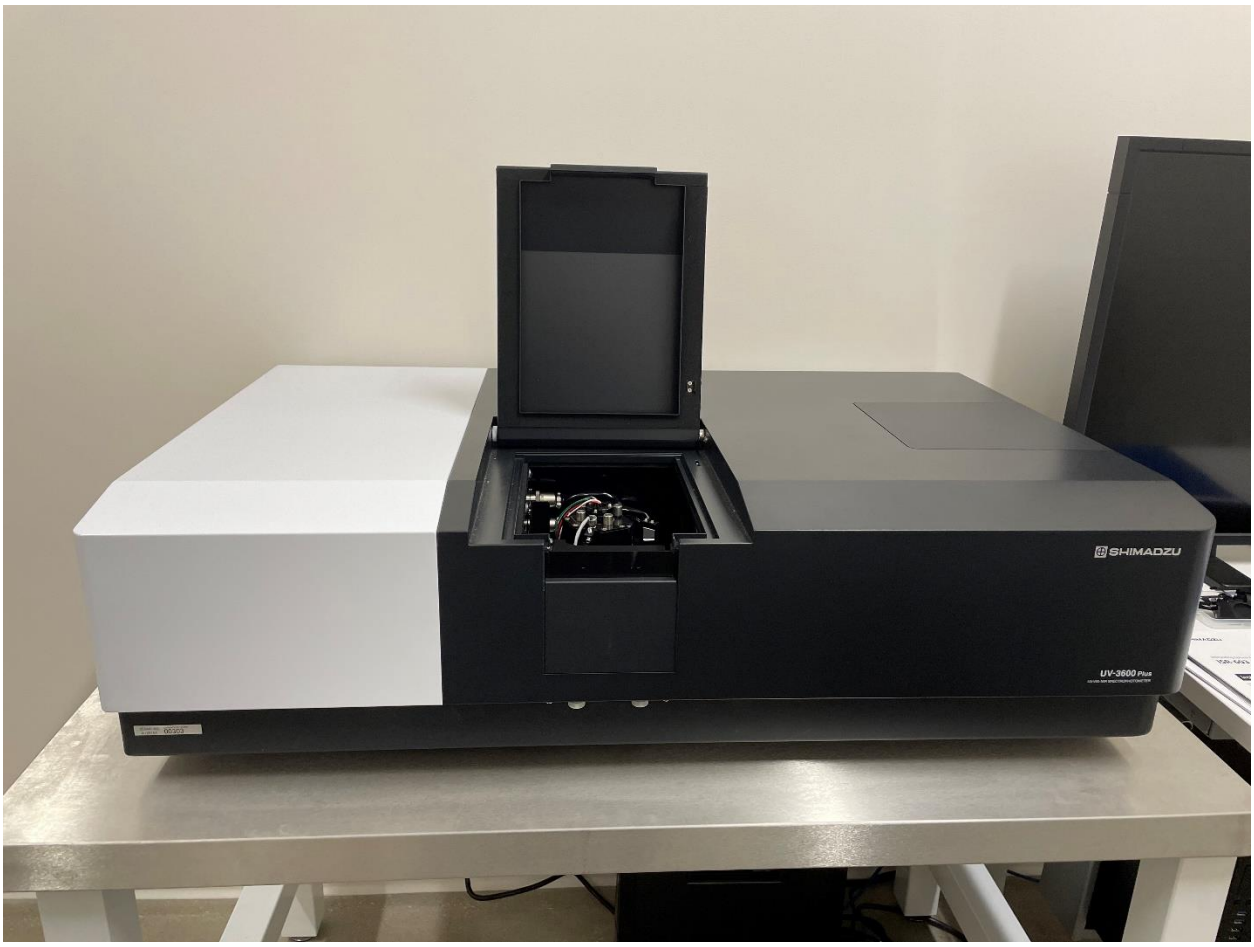

Figure 27: Shimadzu UV-Vis 3600-Plus.

The baseline for reflection mode was a freshly evaporated silver film about 500 nm thick on cleaned Corning glass. The scans are performed at a gradual speed between 350 and 800 nanometers, with a step size of 1.0 nanometers and a slit width of 2.0 nanometers. After drying the samples in a gentle flow of dry nitrogen, samples that had been exposed to degassed and non-degassed water for fixed periods of time were calculated. In-situ tests are carried out on Ag nanorods that have been stored within polycarbonate cuvettes. A 500 nm silver film is deposited onto the inner back side of a polycarbonate cuvette as a baseline, and the cuvette is sealed with degassed water to prevent the fresh film from corroding too quickly. The cuvettes are masked with Kapton tape to avoid deposition onto the other internal or external sides of the cuvette, which is discarded after deposition. Following that, cuvettes with Ag nanorods accumulated on the interior back side are weighed directly after being filled with degassed or non-degassed vapor. Then, at predetermined times, measurements are taken to detect time-dependent variations in reflective spectra.

Raman Spectroscopy

Raman spectroscopy was conducted on Ag nanorod samples sensitized in an aqueous solution of 10-5 M R6G. R6G solution was made by mixing a sufficient volume of R6G powder into degassed and non-degassed water and actively stirring for one hour. To keep air from dissolving into the mixture, the degassed solution was made by swirling the mixing solution when under light vacuum. The samples were immersed in the solutions for 12 hours before being rinsed five times with degassed deionized water and dried under a gentle nitrogen flow. A Horiba T64000 Raman Spectrometer with microscope functionality and a liquid nitrogen cooled CCD detector was used. A 10 X Olympus objective was used to focus the 532 nm laser to a ~10 μm spot on the surface of the sample. The laser power is limited to ten watts. The spectrometer's

entry slit is set to 200 m. With 25 accumulations per spectrum, the accumulation period is set to 1 second. For each measurement, 10 scans are taken over a spectral array of 250 to 2250 wavenumbers.

Chapter 5. Results

One of the characteristics that attract research in the nanometer scale is material properties change from the bulk material. An example of optical characteristics changing is when gold is in bulk material it tends to be a shiny yellow color, while in the nanoparticle range, golds changes color. Nanotechnology helps the ability for a material like cloth to become less wet and dirty or a frying pan to become stick resistant. The goal of this investigation is to measure oxidation and sulfurization on air exposed nanoscale samples, H_20 exposed nanoscale samples, and H_20 degassed exposed nanoscale samples, then see how these measures affect spectra in Raman spectroscopy.

Results

First, we present the morphological and chemical changes of the Ag nanorods after exposure for 168 hours to air, degassed water, and non-degassed water, Figure 28.

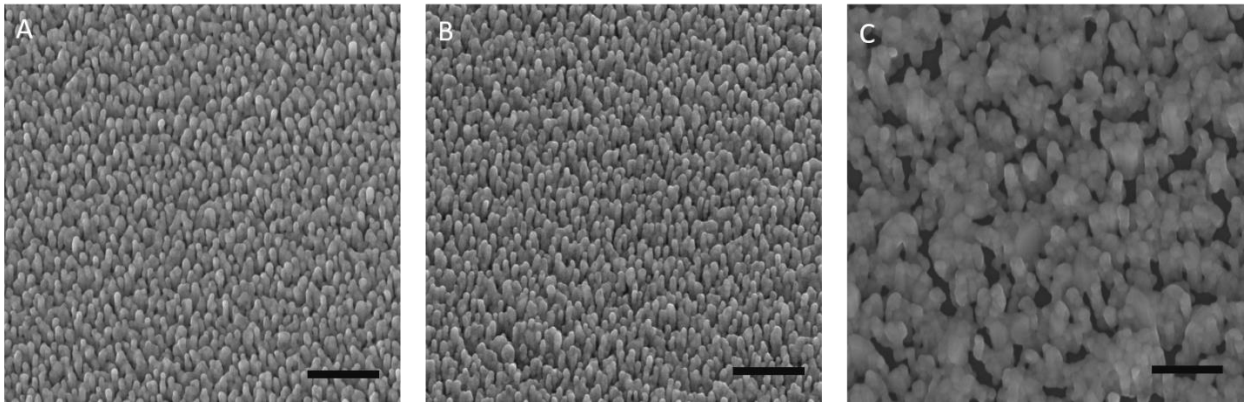

Figure 28: SEM image of Ag nanorods after exposure to (A) air, (B) degassed di-ionized water, and (C) non-degassed di-ionized water for 168 hours. The scale bars are 500 nm.

The time of 168 hours is chosen to get visible changes in morphology. No appreciable difference is observable between the samples stored in air or degassed water. However, the sample stored in non-degassed water exhibits significant coarsening and loss of nanorod morphology. Additional microscopy was performed on sets after one hour and 12 hours and visible morphology changes, not shown here, which shows similar but less obvious differences. In passing, we note that EDS was also performed on the samples of Figure 28. Although the results cannot be directly interpreted due to beam penetration differences with varying density and chemical composition, qualitative results indicate an insignificant difference in oxygen between samples in air and degassed water and a significant increase in the non-degassed sample. From the regular water EDS spectrum shown in Figure 29, we see approximately 20 weighted percent of oxygen and no identifiable sulfur peaks.

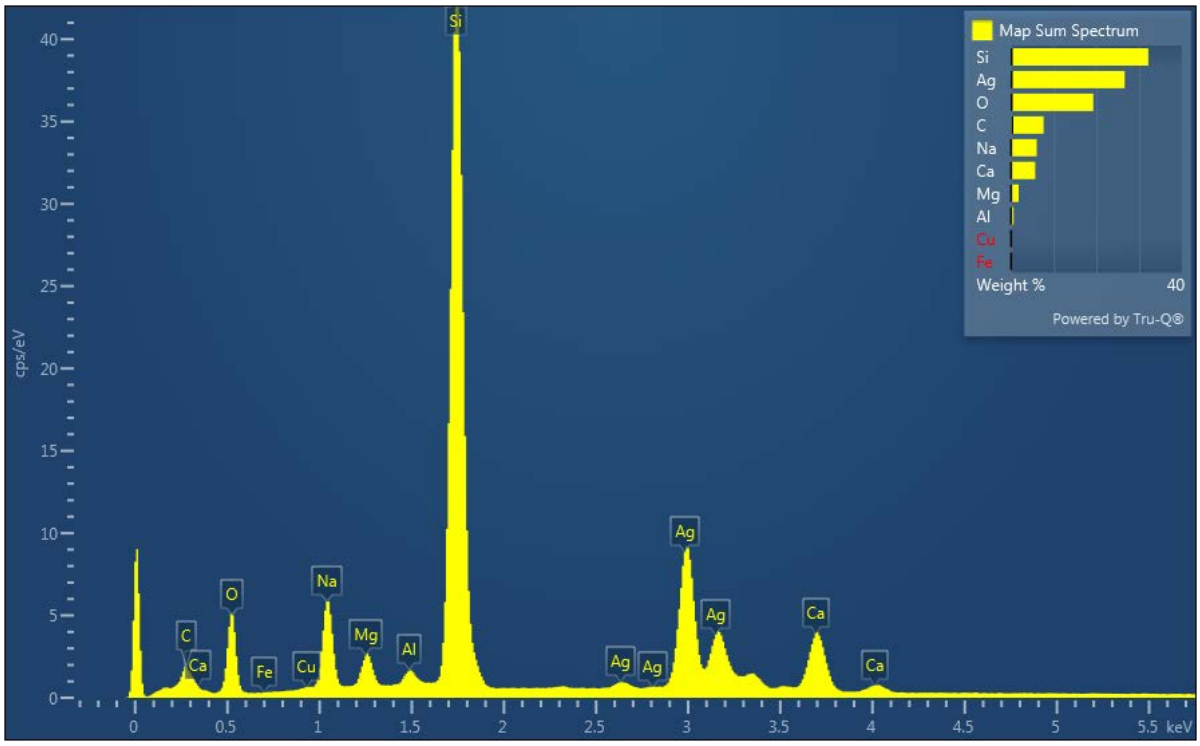

Quant Results View

Viewed Data: Map Sum Spectrum

Processing Option Used: All Elements Processed (Normalized)

Element	Wt%	Wt% Sigma
C	7.62	0.30
O	19.24	0.15
Na	6.03	0.05
Mg	1.79	0.03
Al	0.63	0.02
Si	32.12	0.14
Ca	5.69	0.05
Fe	0.13	0.04
Cu	0.15	0.05
Ag	26.61	0.14
Total	100.00	

Figure 29: SEM spectrum of Ag nanorods after exposure to non-degassed di-ionized water for 168 hours.

From the degassed water EDS spectrum shown in Figure 30, we see again approximately 20 weighted percent of oxygen and no identifiable sulfur peaks. This indicates that the primary species of corrosion is oxidation and not sulphurization as in air.

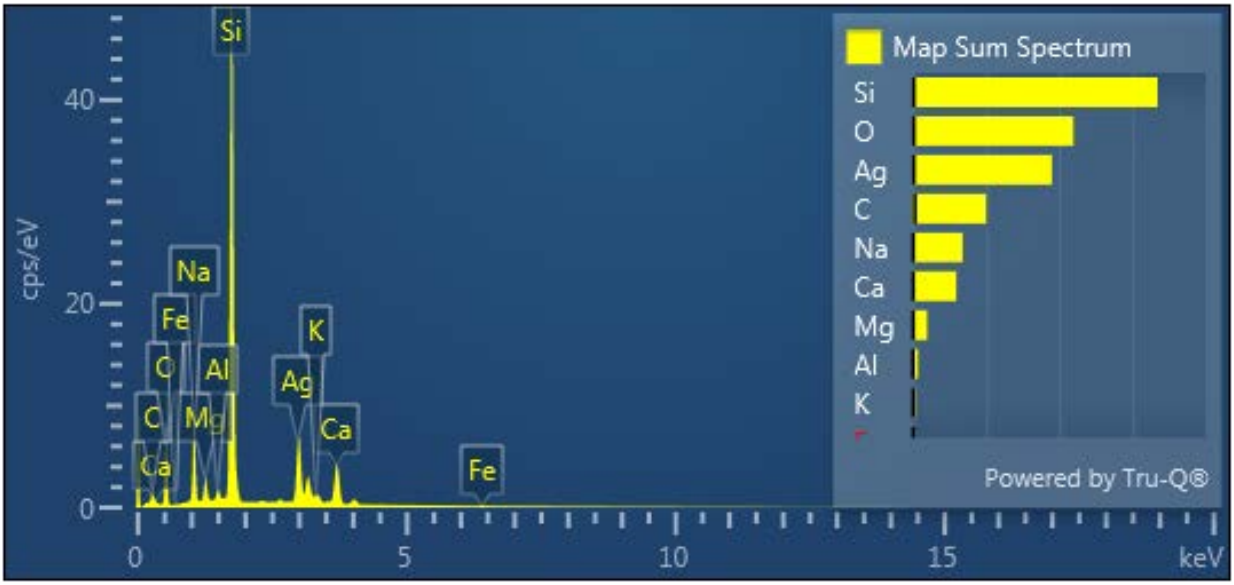

Quant Results View

Viewed Data: Map Sum Spectrum

Processing Option Used: All Elements Processed (Normalized)

Element	Wt%	Wt% Sigma
C	9.97	0.29
O	21.90	0.13
Na	6.75	0.04
Mg	1.90	0.02
Al	0.68	0.02
Si	33.40	0.13
K	0.37	0.02
Ca	5.90	0.04
Fe	0.14	0.03
Ag	18.98	0.10
Total	100.00	

Figure 30: SEM spectrum of Ag nanorods after exposure to degassed di-ionized water for 168 hours.

We present the changes in optical response caused by the exposure to the varied conditions, Figure 31. Samples exposed to air for 12 hours are observed to have multiple absorption peaks and a strong absorption, owing to surface plasmon resonance excitation, centered around ~400nm. Likewise, after exposure to degassed di-ionized water, labeled DG H2O in Figure 31, the intensity of absorption decreases but peak locations are unchanged. Alternatively, after exposure to non-degassed water for 12 hours, labeled H2O in Figure 31, the Ag nanorods do not exhibit any of the secondary peaks and there is a significant decrease in the intensity of and blue shift of the main resonance peak. Surface plasmon resonance is considered to be the dominating factor in most sensing applications using Ag nanorods, and the decrease in resonance peak is expected to result in a decrease in sensing activity [44].

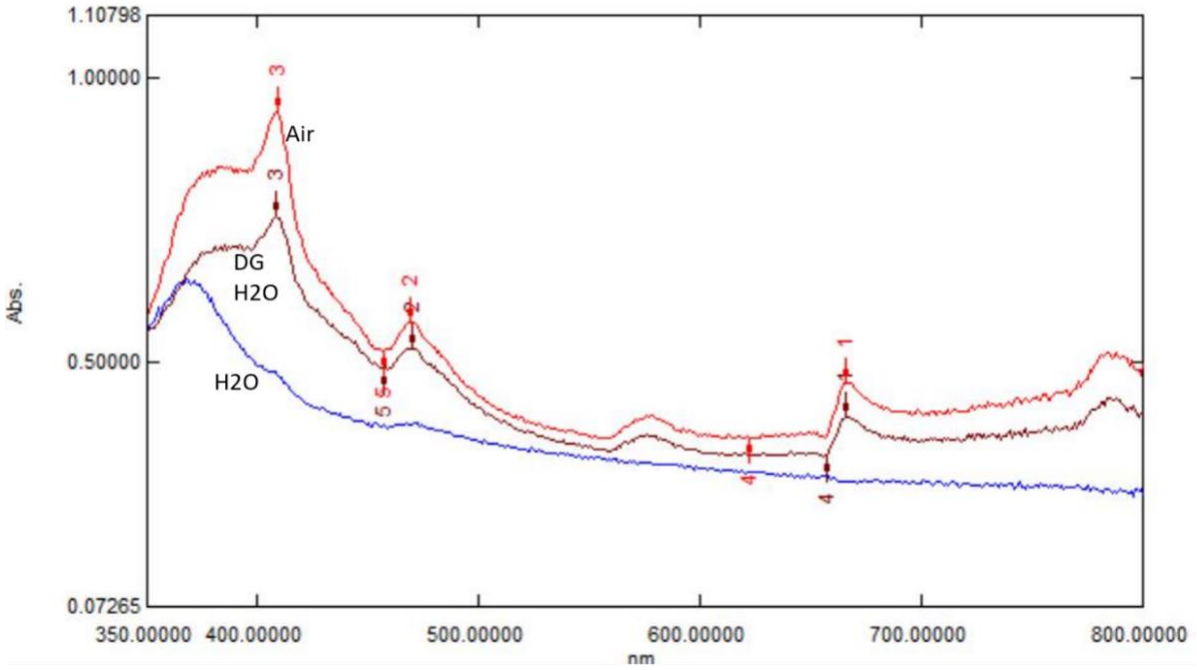

Figure 31: UV-Vis reflection spectra for Ag nanorod samples exposed to varied conditions for 12 hours.

Next, we present the results of a time resolved in-situ experiment measuring the optical reflectance of Ag nanorods deposited inside a cuvette exposed to non-degassed water, Figure 32.

Scans are taken every 10 minutes over the course of one hour, progressing in the direction of the arrow on Figure 32. It is noted that even within only one hour there is an observable change in reflective spectrum. This is significant as the area of decrease overlaps with the commonly used Raman laser lines of 473nm and 524nm, which may lead to changes in measured Raman signals.

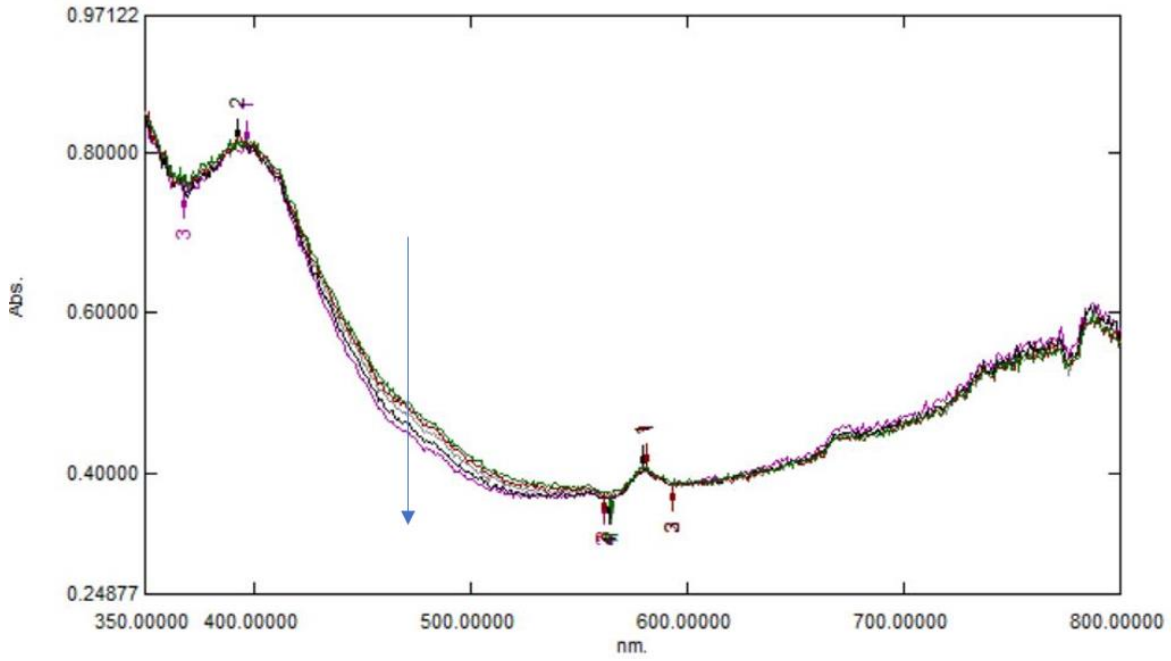

Figure 32: Time resolved UV-Vis reflection spectra for a Ag nanorod sample exposed to non-degassed di-ionized water. Spectra are taken every 10 minutes over one hour and progress in the direction of the arrow.

Raman spectroscopy is also performed and presented in Figure 33, 34, and 35 to correlate changes in the morphology, optical response, and performance as a sensor. 9 spectra each were measured on a sample exposed to non-degassed R6G solution for 12 hours, labeled H2O in Figure 33, and a second sample in degassed R6G solution for 12 hours, labeled DG H2O in Figure 33.

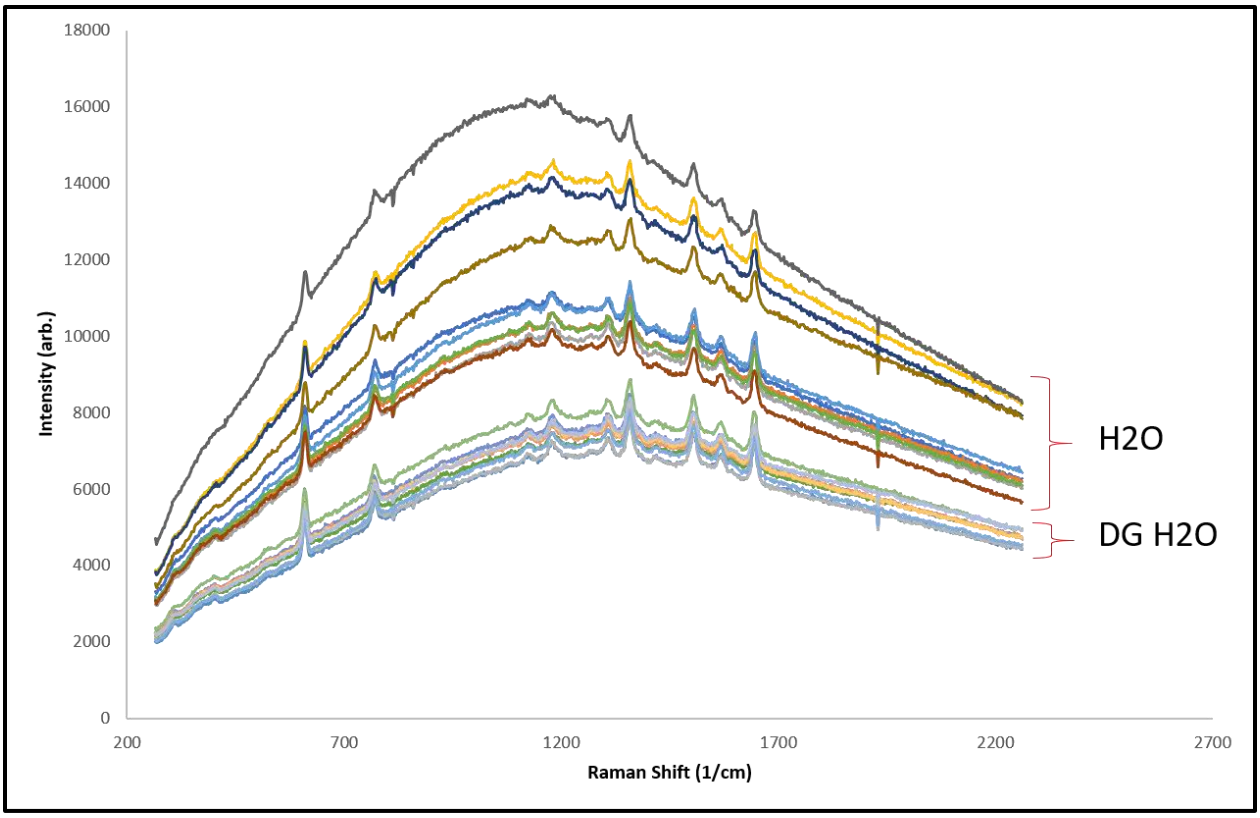

Figure 33: Raman spectra of Ag nanorods sensitized with R6G solution in non-degassed de-ionized water, labeled H2O, and degassed water, labeled DG H2O.

While the overall Raman signal is stronger for the same in non-degassed solution, shown in Table 1, the measured peak to background ratios of both groups of measurements do not have statistically significant variation which is shown in Table 2.

Table 1: Raw Peak counts used for the background ratio from the R6G regular and degassed water samples

Raw Peaks Used for Ratio	R6G Regular H2O	R6G DO H2O
	11319.00	7756.25
	10989.40	8032.75
	10847.00	8479.13
	14593.00	8174.75
	11428.40	7842.25
	10897.60	8340.50
	14090.90	8066.25
	10389.30	8874.75
	15772.30	8378.75
Average	13063.30	8216.15
Standard Deviation	1893.20	345.32

We hypothesize that the corrosion of the Ag nanorods is primarily in the form of oxidation, which has been demonstrated to produce significant increases in metal-enhanced fluorescence in the literature. Further, the spread of spectral intensities from the non-degassed sample is approximately double that of the degassed sample shown in Table 2.

Table 2: Peak to background ratio from the R6G regular and degassed water samples

Peak to Background Ratio	R6G Regular H2O	R6G DO H2O
	1.13	1.13
	1.13	1.13
	1.14	1.15
	1.10	1.13
	1.13	1.14
	1.13	1.14
	1.10	1.14
	1.13	1.14
	1.10	1.14
Average	1.12	1.14
Standard Deviation	0.02	0.01
Std. Dev. % (Scatter)	1.79%	0.88%

Spectral scatter and non-repeatability have been observed and discussed in detail for Raman spectroscopy using nanostructured substrates in the literature [41]. Hypothesized to be intrinsic to the non-periodic structure of the Ag nanorods grown from PVD, a significant contribution from rapid corrosion has likely been overlooked.

Another batch of specimens were run with caffeine as the analyte. 6 spectra each were measured on a sample exposed to non-degassed caffeine solution for 12 hours, labeled regular H2O in Figure 34, and a second sample in degassed caffeine solution for 12 hours, labeled Deoxygenated (DO) H2O in Figure 35.

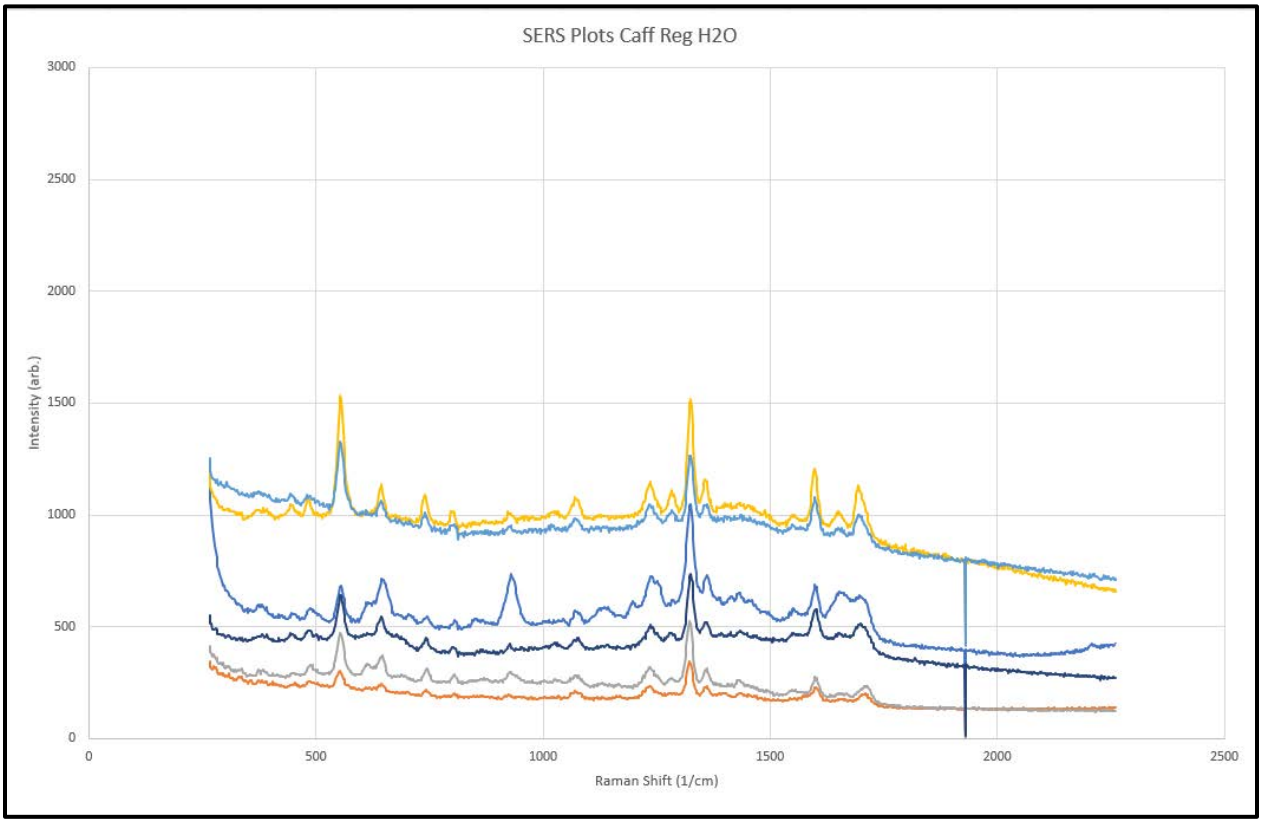

Figure 34: Raman spectra of Ag nanorods sensitized with Caffeine solution in regular non-degassed de-ionized water, labeled Reg H2O.

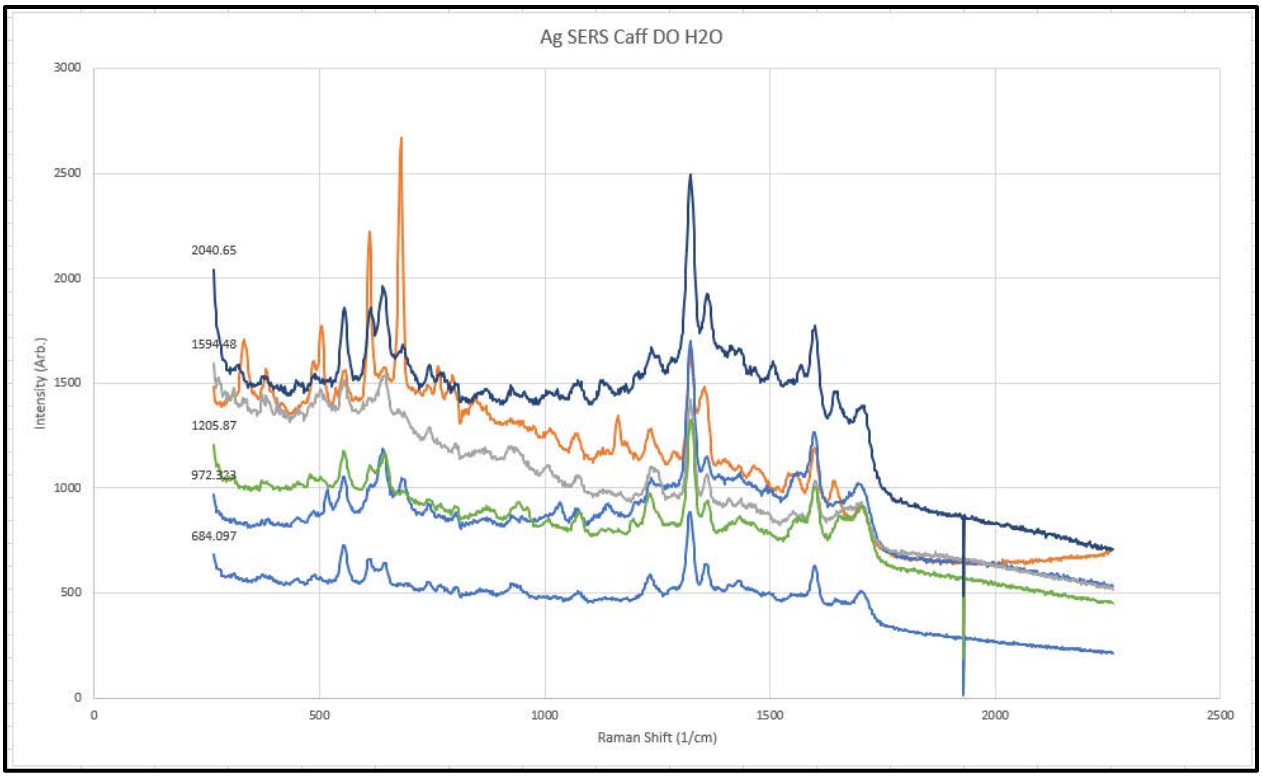

Figure 35: Raman spectra of Ag nanorods sensitized with caffeine solution in deoxygenated water, labeled DO H2O.

A non-resonant molecule loses nearly 50% of signal when regular water is used and corrodes the sample compared to degassed water by results shown in Table 3.

Table 3: Raw Peak counts used for the background ratio from the caffeine regular and deoxygenated water samples

Raw Peaks Used for Ratio	Caffeine Regular H2O	Caffeine DO H2O
	1045.94	1645.48
	335.65	1688.65
	513.03	1423.13
	1519.45	887.097
	1264.35	1325.94
	734.23	2488
Average	902.11	1656.86
Standard Deviation	454.63	631.40

In both data sets from R6G and the caffeine measurements corrosion plays a drastic significance in the increase of scatter shown in Table 4. This indicates that the presence of dissolved gases in water used for SERS substrate sensitization is significant and critical to real world applications.

Table 4: Peak to background ratio from the caffeine regular and deoxygenated water samples

Peak to background ratio	Caffeine Regular H2O	Caffeine DO H2O
	1.74	1.45
	1.68	1.62
	2.17	1.54
	1.44	1.73
	1.27	1.62
	1.59	1.53
Average	1.65	1.58
Standard Deviation	0.31	0.10
Std. Dev. % (Scatter)	18.79%	6.33%

Finally, we present SPM measurements of the samples. Five sample were measured using the SPM in contact mode. The first set of samples were measured immediately after removal from vacuum and represent a clean baseline. Next, the measurements were repeated with a set of five samples that were submerged in non-degassed water for two hours. A representative comparison of the topographies is shown in Figure 36, where the baseline sample is on the left and the submerged sample is on the right. It is evident from the topographical images that even brief exposure to water with dissolved gases results in rapid and dramatic morphological changes to the surfaces.

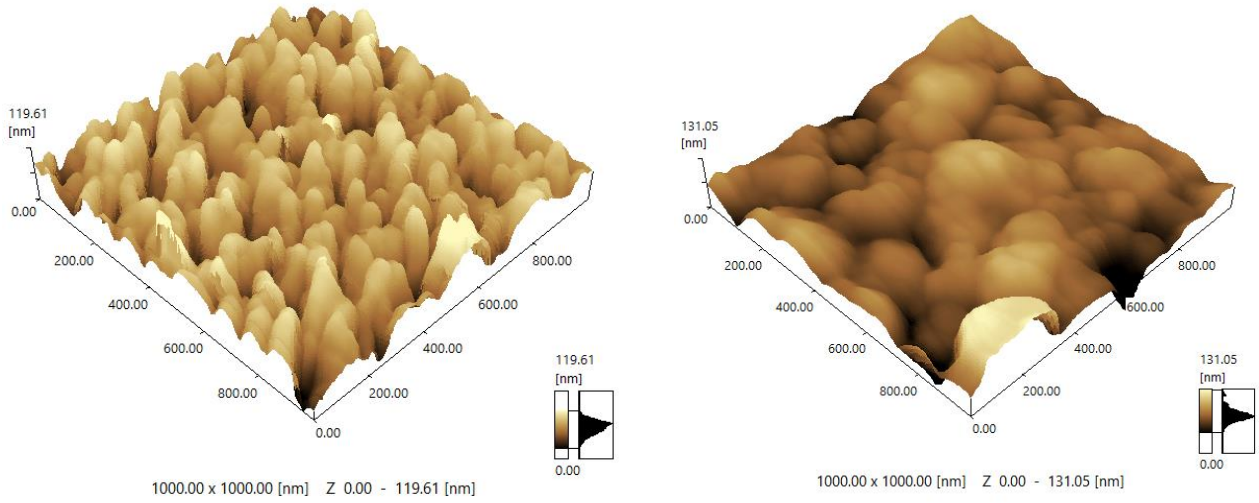

Figure 36: Left: Baseline Ag nanorods topography correlative to the SEM imaging A in Figure 28. Right: Local imaging of topography for Ag Oxidized Nanorods after sitting in water for 2 hours.

The same samples were analyzed on the SPM using KFM to determine if the surfaces have chemically changed from the baseline state. The baseline, Figure 37 left, shows the potential measured on clean Ag surfaces without significant oxidation or corrosion. The tips of the nanorods are clearly evident in the potential plot. After soaking in the non-degassed water for two hours the average surface potential, shown on the right of Figure 37, increases to greater than 3.0V and there is no evidence for the presence of fine nanorod tips. Based on the measured change in surface potential, the authors hypothesize that the surfaces of the nanorods have undergone oxidation in the non-degassed water. This hypothesis will be tested with future transmission electron microscopy (TEM) analyses.

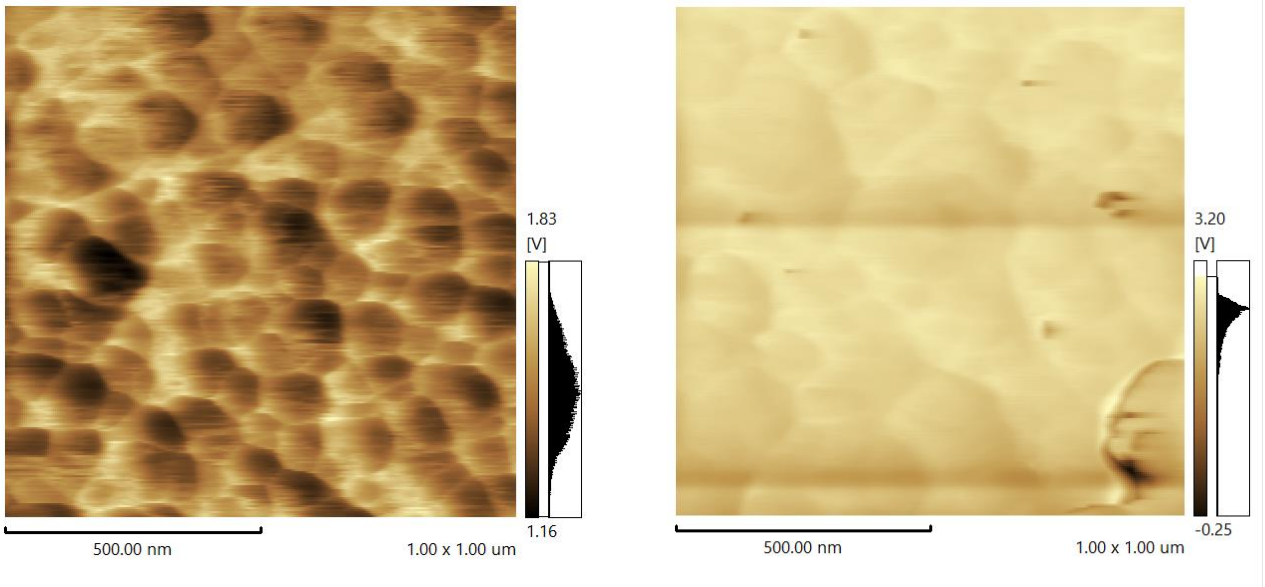

Figure 37: Left: Ag nanorods surface potential contour map taken immediately after removal from vacuum. Right: Ag nanorod surface potential contour map taken after submersion in non-degassed water for two hours.

Chapter 6. Conclusion and Future Work

Conclusion

This document reports on the corrosion of Ag nanorods by dissolved gasses present in de-ionized water, which is commonly used in many nanomaterial sensing experiments without any consideration. Through SEM, UV-Vis reflection, Raman, and SPM characterization it is evident that dissolved gasses in water cause significant corrosion in Ag nanorods, leading to significant morphological and optical response changes on the timescale of hours. SERS experiments were performed, and it is demonstrated that the resonant state of the molecule and the fluorescent action lead to significant differences. A fluorescent molecule is observed to have greater raw SERS signal but significantly higher relative spot to spot deviation in signal. These results motivate further investigation into the underlying mechanisms dominating observed spectral changes in nanostructured metals when they are used as biological sensors. Decoupling of

spectral changes caused by experimental artifact and unanticipated mechanisms is essential to improving these sensing technologies. A non-resonant molecule loses nearly 50% of signal when regular water is used compared to degassed water. This indicates that the presence of dissolved gases in water used for SERS substrate sensitization is significant and critical to real world applications.

After looking at the results between our fluorescent R6G molecule and our non-resonant caffeine molecules, the data suggests when performing SERS analysis, the use of DO water is beneficial. For a resonant molecule, like glycoprotein found in SARS-CoV-2, you may not want to using DO water, so oxidation can occur on your samples to activate metal enhanced fluorescence, which in-turn increases Raman raw count signal intensity, seen in our R6G results from Table 1. However, oxidation introduces statistically significant scatter for both resonant and non-resonant molecule being analyzed. Therefore, when using DO water with our substrate-sample detecting resonant molecules you still have raw count peaks, shown in Table 1, with significantly less scatter as shown in Tables 1 and Table 2. When using DO water with our substrate-sample detecting non-resonant molecules, like our caffeine, the data indicates significantly higher raw count of Raman signal, shown in Table 3 and Table 4, and significantly less scatter shown in Table 4. Theoretically, in the future, research can be conducted with instrumentation to better understand how to control oxidation for Raman samples, which would likely help optimize results for SERS analysis.

Future Work

With more time and resources, there are two good ways to characterize the substrate SERS phenomenon and oxidation species, (1) by Grazing Incidence X-Ray Diffractometry (GIXRD) and (2) by examination with Transmission Electron Microscopy (TEM). In GIXRD,

the thin film sample stage, monochromator, and suction pump are all part of this customized system. The penetration of incident X-rays onto the substrate sample is restricted as much as possible, grazing off the surface, by using the defined incidence angle, parallel X-ray diffractometry process, resulting in low background, thin film X-ray diffraction patterns which will report oxidation species.

TEM uses an electron elimination source beam that creates the image of a specimen. In the case of TEM, the sample analyzed is typically is thin films where the electron being accelerated towards the sample are transmitted through the sample, rather than the similar SEM where this has a thicker sample and the electrons bounce off the sample to the detector. The electrons beam targeting the sample in TEM are of short wavelengths therefore enabling ease of transmission through the sample. These short-wavelength electrons are then scattered by different structural properties of the sample which can then be captured by the detector to create a high resolution picture of the ultra thin sample. The detector will additionally allow for understanding of morphologic, crystallographic, and compositional aspects of the specimen. TEM uses high velocity electrons through a vacuum chamber to clear the disruptive air molecules which allows for resolutions of the less than 10 nanometer scale images of specimen. The TEM gives the power to visualize atoms and analyze oxidation species to further understand the corrosion of Ag nanorods of SERS substrates. With TEM we will analyze with two different mechanisms, HR Imaging and Electron Energy Loss Spectroscopy (EELS).

We'll use high-resolution imagery to see how the thickness of the film that forms on the surface affects the local surface morphology. We'll search for improvements in surface roughness of a few nanometers that could lead to increased analyte adhesion and surface area due to oxidation. Increased surface roughness and more area for the analyte to attach to are likely

duel and confounding results of reduced EM output due to the oxide layer, but also increased surface roughness and more area for the analyte to attach to.

We'll also use EELS (electron energy loss spectroscopy) to assess the chemical composition of the very thin surface layers selected area diffraction (SAD) to describe the crystalline structure at the surface. We'll also look for a thin organic film on the top, which may indicate organic contaminants in the water. Which also eliminates the possibility that some of the Sulphur compounds in the water are causing degradation at the same time. We'll also look at whether oxidation can be advantageous. Will the oxide, for example, act as an inert shielding coating on the nanorods to prevent Sulphur or other atmospheric compounds from corroding them? XPS and AES are two other approaches we considered but opted against. Both of these techniques necessitate baking the specimen, which alters the structure and can allow any of the attached materials to escape to the surface.

References

1. Karabacak T, Wang G, Lu T. Physical self-assembly and the nucleation of three-dimensional nanostructures by oblique angle deposition. *Journal of Vacuum Science & Technology A: Vacuum, Surfaces, and Films*. 2004(22).

2. Robbie K BM. Sculptured thin films and glancing angle deposition: Growth mechanics and applications. *Journal of Vacuum Science & Technology*. 1997(15).

3. Robbie K, Sit J, Brett M. Advanced techniques for glancing angle deposition. *Journal of Vacuum Science and Technology*. 1998(16).

4. Prosolov KA, Belyavskaya OA, Linders J, et al. Glancing angle deposition of zn-doped calcium phosphate coatings by RF magnetron sputtering. *Coatings (2079-6412)*. 2019;9(4):220. http://search.ebscohost.com/login.aspx?direct=true&AuthType=shib&db=edb&AN=136165025&site=eds-live&scope=site&custid=s6281220.

5. Zhang X, Cai S, You D, et al. Template-free sol-gel preparation of superhydrophobic ORMOSIL films for double-wavelength broadband antireflective coatings. *Advanced Functional Materials*.2014;23(35):4361. http://search.ebscohost.com/login.aspx?direct=true&AuthType=shib&db=edb&AN=90469986&site=eds-live&scope=site&custid=s6281220.

6. Volpian O, Kuzmichev A. Nanogradient optical coatings. *Russian Journal of General Chemistry*.2013;83(11):2182. http://search.ebscohost.com/login.aspx?direct=true&AuthType=shib&db=edb&AN=93255199&site=eds-live&scope=site&custid=s6281220.

7. Diwan A, Singh B, Roychowdhury T, et al. Porous, high capacity coatings for solid phase microextraction by sputtering. *Anal Chem*. 2016;88(3):1593. http://search.ebscohost.com/login.aspx?direct=true&AuthType=shib&db=edb&AN=113223864&site=eds-live&scope=site&custid=s6281220.

8. Shanmugam N, Pugazhendhi R, Madurai Elavarasan R, Kasiviswanathan P, Das N. Anti-reflective coating materials: A holistic review from PV perspective. *Energies (19961073)*. 2020;13(10):2631. http://search.ebscohost.com/login.aspx?direct=true&AuthType=shib&db=edb&AN=143637608&site=eds-live&scope=site&custid=s6281220.

9. Yilmaz M. Silver-nanoparticle-decorated gold nanorod arrays via bioinspired polydopamine coating as surface-enhanced raman spectroscopy (SERS) platforms. *Coatings (2079-6412)*. 2019;9(3):198. http://search.ebscohost.com/login.aspx?direct=true&AuthType=shib&db=edb&AN=135683486&site=eds-live&scope=site&custid=s6281220.

10. Khan SB, Wu H, Li J, Chen L, Zhang Z. Bilayer SiO2 nanorod arrays as omnidirectional and thermally stable antireflective coating. *Advanced Engineering Materials*. 2018;20(5):1. http://search.ebscohost.com/login.aspx?direct=true&AuthType=shib&db=edb&AN=129857422&site=eds-live&scope=site&custid=s6281220.

11. Zgheib E, Alhussein A, Slim MF, Khalil K, François M. Elastic behavior of anisotropic coatings sputter-deposited at oblique incidence. *Int J Mech Sci*. 2020. http://search.ebscohost.com/login.aspx?direct=true&AuthType=shib&db=edselp&AN=S0020740320311462&site=eds-live&scope=site&custid=s6281220.

12. Khan SB, Zhang Z, Lee SL. Single component: Bilayer TiO2 as a durable antireflective coating. *J Alloys Compounds*. 2020;834. http://search.ebscohost.com/login.aspx?direct=true&AuthType=shib&db=edselp&AN=S0925838820315000&site=eds-live&scope=site&custid=s6281220.

13. Stephen Stagon. *Physical vapor deposition of nanorods from science to technology*. University of Connecticut; 2013.

14. Taguchi A, Saito Y, Watanabe K, Yijian S, Kawata S. Tailoring plasmon resonances in the deep-ultraviolet by size-tunable fabrication of aluminum nanostructures. *Appl Phys Lett*. 2012;101(8). http://search.ebscohost.com/login.aspx?direct=true&AuthType=shib&db=edswsc&AN=000308420800010&site=eds-live&scope=site&custid=s6281220. doi: 10.1063/1.4747489.

15. Ray K, Chowdhury MH, Lakowicz JR. Aluminum nanostructured films as substrates for enhanced fluorescence in the ultraviolet-blue spectral region. *ANALYTICAL CHEMISTRY - WASHINGTON DC-*. 2007(17): 6480. http://search.ebscohost.com/login.aspx?direct=true&AuthType=shib&db=edsbl&AN=RN216435586&site=eds-live&scope=site&custid=s6281220.

16. Weiss A, Haran G. Time-dependent single-molecule raman scattering as a probe of surface dynamics. *J Phys Chem B*. 2001(49): 12348. http://search.ebscohost.com/login.aspx?direct=true&AuthType=shib&db=edsggo&AN=edsgcl.83454429&site=eds-live&scope=site&custid=s6281220.

17. Xu X, Kim K, Liu C, Fan D. Fabrication and robotization of ultrasensitive plasmonic nanosensors for molecule detection with raman scattering. *Sensors*. 2015;15(5):10422-10451. http://search.ebscohost.com/login.aspx?direct=true&AuthType=shib&db=edsdoj&AN=edsdoj.bcd294591f24784ae3b1fbaf7b5fe7e&site=eds-live&scope=site&custid=s6281220. doi: 10.3390/s150510422.

18. Bosnick KA, Jiang J, Brus LE. Fluctuations and local symmetry in single-molecule rhodamine 6G raman scattering on silver nanocrystal aggregates. *J Phys Chem B*. 2002;106(33):80968099. http://search.ebscohost.com/login.aspx?direct=true&AuthType=shib&db=edswsc&AN=000177472800017&site=eds-live&scope=site&custid=s6281220. doi: 10.1021/jp0256241.

19. Michaels AM, Jiang J, Brus L. Ag nanocrystal junctions as the site for surface-enhanced raman scattering of single rhodamine 6G molecules. *J Phys Chem B*. 2000(50): 11965. http://search.ebscohost.com/login.aspx?direct=true&AuthType=shib&db=edsggo&AN=edsgcl.124191208&site=eds-live&scope=site&custid=s6281220.

20. Jiang J, Bosnick K, Maillard M, Brus L. Single molecule raman spectroscopy at the junctions of large ag nanocrystals. *J Phys Chem B*. 2003(37):
9964. http://search.ebscohost.com/login.aspx?direct=true&AuthType=shib&db=edsbl&AN=RN137719069&site=eds-live&scope=site&custid=s6281220.

21. Xu H, Aizpurua J, Kall M, Apell P. Electromagnetic contributions to single-molecule sensitivity in surface-enhanced raman scattering. *PHYSICAL REVIEW -SERIES E-*. 2000(3):
4318. http://search.ebscohost.com/login.aspx?direct=true&AuthType=shib&db=edsbl&AN=RN085223021&site=eds-live&scope=site&custid=s6281220.

22. Maruyama Y, Futamata M. Elastic scattering and emission correlated with single-molecule SERS. *J Raman Spectrosc*. 2005(6):
581. http://search.ebscohost.com/login.aspx?direct=true&AuthType=shib&db=edsbl&AN=RN171017474&site=eds-live&scope=site&custid=s6281220.

23. Xu H, Bjerneld EJ, Kaell M, Boerjesson L. Spectroscopy of single hemoglobin molecules by surface enhanced raman scattering. *Phys Rev Lett*. 1999(21):
4357. http://search.ebscohost.com/login.aspx?direct=true&AuthType=shib&db=edsbl&AN=RN070623675&site=eds-live&scope=site&custid=s6281220.

24. De Gelder J, De Gussem K, Vandenabeele P, Moens L. Reference database of raman spectra of biological molecules. *J Raman Spectrosc*. 2007(9):
1133. http://search.ebscohost.com/login.aspx?direct=true&AuthType=shib&db=edsbl&AN=RN214683116&site=eds-live&scope=site&custid=s6281220.

25. Jha SK, Ahmed Z, Agio M, Ekinci Y, Loffler JF. Deep-UV surface-enhanced resonance raman scattering of adenine on aluminum nanoparticle arrays. *JOURNAL- AMERICAN CHEMICAL SOCIETY*. 2012(4):
1966. http://search.ebscohost.com/login.aspx?direct=true&AuthType=shib&db=edsbl&AN=RN309255676&site=eds-live&scope=site&custid=s6281220.

26. Brant E. Billinghurst, Sulayman A. Oladepo, Glen R. Loppnow. pH-dependent UV resonance raman spectra of cytosine and uracil. *J Phys Chem B*. 2009;113(20):7392-7397
. http://search.ebscohost.com/login.aspx?direct=true&AuthType=shib&db=aci&AN=39988098&site=eds-live&scope=site&custid=s6281220. doi: 10.1021/jp811327w.

27. Kneipp K, Kneipp H, Bhaskaran Kartha V, et al. Detection and identification of a single DNA base molecule using surface-enhanced raman scattering (SERS). *PHYSICAL REVIEW -SERIES E-*. 1998(6):R6281
. http://search.ebscohost.com/login.aspx?direct=true&AuthType=shib&db=edsbl&AN=RN046073540&site=eds-live&scope=site&custid=s6281220.

28. Kneipp K, Kneipp H, Bhaskaran Kartha V, et al. Detection and identification of a single DNA base molecule using surface-enhanced raman scattering (SERS). *PHYSICAL REVIEW -SERIES E-*. 1998(6):R6281

29. Tsang, J. C., J. R. Kirtley, and J. A. Bradley. "Surface-enhanced Raman spectroscopy and surface plasmons." Physical review letters 43.11 (1979): 772.

30. Stiles PL, Dieringer JA, Shah NC, Van Duyne R,P. Surface-enhanced raman spectroscopy. Annu Rev Anal Chem (Palo Alto Calif). 2008;1:601-626.

31. Moskovits, Martin. "Surface-enhanced Raman spectroscopy: a brief retrospective." Journal of Raman Spectroscopy: An International Journal for Original Work in all Aspects of Raman Spectroscopy, Including Higher Order Processes, and also Brillouin and Rayleigh Scattering 36.6-7 (2005): 485-496.

32. Wang H, Hogan CA, Miller JA, Sahoo MK, Huang C, Mfuh KO, et al. Performance of nucleic acid amplification tests for detection of severe acute respiratory syndrome coronavirus 2 in prospectively pooled specimens. Emerg Infect Dis. 2012 Jan 11/20/2020.

33. Tadesse LF, Safir F, Ho C, et al. Toward rapid infectious disease diagnosis with advances in surface-enhanced raman spectroscopy. J Chem Phys. 2020;152(24):1-14.

34. Zhong J, Roesch EL, Viereck T, Schilling M, Ludwig F. Rapid and sensitive detection of SARS-CoV-2 with functionalized magnetic nanoparticles. 2020.

35. Shanmukh, Saratchandra, et al. "Rapid and sensitive detection of respiratory virus molecular signatures using a silver nanorod array SERS substrate." Nano letters 6.11 (2006): 2630-2636.

36. Hill, Ryan T. "Plasmonic biosensors." Wiley Interdisciplinary Reviews: Nanomedicine and Nanobiotechnology 7.2 (2015): 152-168.

37. Kabashin AV, Evans P, Pastkovsky S, et al. Plasmonic nanorod metamaterials for biosensing. Nature Materials. 2009;8(11):867-871

38. Xu H, Bjerneld EJ, Kaell M, Boerjesson L. Spectroscopy of single hemoglobin molecules by surface enhanced raman scattering. Phys Rev Lett. 1999(21): 4357.

39. Michaels AM, Jiang J, Brus L. Ag nanocrystal junctions as the site for surface-enhanced raman scattering of single rhodamine 6G molecules. J Phys Chem B. 2000(50): 11965.

40. Bachenheimer L, Scherzer R, Elliott P, Stagon S, Gasparov L, Huang H. Degradation mechanism of g nanorods for surface enhanced raman spectroscopy. *Scientific Reports*. 2017;7(1):1-4. . doi: 10.1038/s41598-017-16580-2.

41. Li D, Yao D, Li C, et al. Nanosol SERS quantitative analytical method: A review. *Trends in Analytical Chemistry*. 2020;127. doi: 10.1016/j.trac.2020.115885.

42. Pedersen KB, Sriramula S, Chhabra KH, Xia H, Lazartigues E. Species-specific inhibitor sensitivity of angiotensin-converting enzyme 2 (ACE2) and its implication for ACE2 activity assays. *American journal of physiology.Regulatory, integrative and comparative physiology*. 2011;301(5):R1293-R1299. doi: 10.1152/ajpregu.00339.2011.

43. Vitko Jr, J., Robert E. Benner, and J. E. Shelby. "Corrosion of thin silver films in an aqueous environment." Solar Energy Materials 9.1 (1983): 51-67.

44. Butler, Ian B., Martin AA Schoonen, and David T. Rickard. "Removal of dissolved oxygen from water: a comparison of four common techniques." Talanta 41.2 (1994): 211-215.

45. Niu X, Stagon SP, Huang H, Baldwin JK, Misra A. Smallest metallic nanorods using physical vapor deposition. Phys Rev Lett. 2013;110(13).

46. Sun, Xiangcheng, et al. "Functionalized aligned silver nanorod arrays for glucose sensing through surface enhanced Raman scattering." RSC Advances 4.45 (2014): 23382-23388.

47. Shimadzu Corporation. SPM-9700-HT.

48. *Chem. Rev.* 2011, 111, 6, 3828–3857. June 8, 2011

49. Uchikoshi, Tetsuo & Itakura, Akiko & Matsunaga, Chika & Ishigaki, Takamasa. (2014). UV Protection Mechanism and Property of Functional Ceramic Particles. Hyomen Kagaku. 35. 45-49. 10.1380/jsssj.35.45.

50. McGregor, Hanna & Wang, Wenbo & Short, Michael & Zeng, Haishan. (2016). Clinical utility of Raman spectroscopy: current applications and ongoing developments. Advanced Health Care Technologies. 13. 10.2147/AHCT.S96486.

51. Zafar MS, Farooq I, Awais M, Najeeb S, Khurshid Z, Zohaib S. Chapter 11 - bioactive surface coatings for enhancing osseointegration of dental implants. In: Kaur G, ed. Biomedical, therapeutic and clinical applications of bioactive glasses. Woodhead Publishing; 2019:313-329. https://www.sciencedirect.com/science/article/pii/B9780081021965000112. https://doi.org/10.1016/B978-0-08-102196-5.00011-2.

52. Imanishi Y, Nakaoka T. Room temperature growth of silver telluride nanorods by sputtering deposition. Appl Phys A. 2018;124(10):1. https://search.ebscohost.com/login.aspx?direct=true&AuthType=shib&db=edsgao&AN=edsgcl.553290025&site=eds-live&scope=site&custid=s6281220. doi: 10.1007/s00339-018-2099-y.

53. Yang J, Lohse S, Boulos S, Murphy C. The early life of gold nanorods: Temporal separation of anisotropic and isotropic growth modes. Journal of Cluster Science. 2012;23(3):799. https://search.ebscohost.com/login.aspx?direct=true&AuthType=shib&db=edb&AN=79194178&site=eds-live&scope=site&custid=s6281220.

54. Lau CN, Xia F, Cao L, Chang H, Gole MT, Murphy CJ. A golden time for nanotechnology. MRS Bull. 2020;45(5):387. https://search.ebscohost.com/login.aspx?direct=true&AuthType=shib&db=edssjs&AN=edssjs.4DFFFD81&site=eds-live&scope=site&custid=s6281220. doi: 10.1557/mrs.2020.119.

55. Harrison H. UF health investigating if new COVID-19 variant has arrived in Jacksonville. First Coast News. Dec 31, 2020. Available from: https://www.firstcoastnews.com/article/news/local/new-covid-19-variant-may-already-be-widespread/77-b61049e2-4061-4830-9bb3-a170aa16350d. Accessed 1/20/21.

56. Ly TN, Park S. High performance detection of alzheimer's disease biomarkers based on localized surface plasmon resonance. Journal of Industrial & Engineering Chemistry.

2020;91:182-190. https://search.ebscohost.com/login.aspx?direct=true&AuthType=shib&db=edo&AN=145755782&site=eds-live&scope=site&custid=s6281220.

57. Lai P, Lu J, Zhang H, et al. The corrosion behavior of M5 (Zr–1Nb-0.12O) alloy in 360 °C water with dissolved oxygen. J Nucl Mater. 2020;532. https://search.ebscohost.com/login.aspx?direct=true&AuthType=shib&db=edselp&AN=S0022311519310347&site=eds-live&scope=site&custid=s6281220. doi: 10.1016/j.jnucmat.2020.152079.

58. Li J, Wang W, Yao Y, Yan C, Han C. Ag nanoparticle-modified silver nanorods for surface enhanced raman scattering. 2018 Cross Strait Quad-Regional Radio Science and Wireless Technology Conference (CSQRWC), Cross Strait Quad-Regional Radio Science and Wireless Technology Conference (CSQRWC), 2018. 2018:1-3. http://search.ebscohost.com/login.aspx?direct=true&AuthType=shib&db=edseee&AN=edseee.8455249&site=eds-live&scope=site&custid=s6281220. doi: 10.1109/CSQRWC.2018.8455249.

59. Ma L, Wang J, Ren C, et al. Detection of corrosion inhibitor adsorption via a surface-enhanced raman spectroscopy (SERS) silver nanorods tape sensor. Sensors and Actuators: B.Chemical. 2020;321. http://search.ebscohost.com/login.aspx?direct=true&AuthType=shib&db=edselp&AN=S0925400520309631&site=eds-live&scope=site&custid=s6281220. doi: 10.1016/j.snb.2020.128617.

60. Xia J, Liu Y, Ran M, Lu D, Cao X, Wang Y. SERS platform based on bimetallic au-ag nanowires-decorated filter paper for rapid detection of miR-196ain lung cancer patients serum. Journal of Chemistry. 2020:1-14. https://search.ebscohost.com/login.aspx?direct=true&AuthType=shib&db=a9h&AN=146585173&site=eds-live&scope=site&custid=s6281220. doi: 10.1155/2020/5073451.

61. Lippi, Giuseppe, Simundic, Ana-Maria and Plebani, Mario. "Potential preanalytical and analytical vulnerabilities in the laboratory diagnosis of coronavirus disease 2019 (COVID-19)" Clinical Chemistry and Laboratory Medicine (CCLM), vol. 58, no. 7, 2020, pp. 1070-1076. https://doi.org/10.1515/cclm-2020-0285

62. Yeh Y, Gulino K, Zhang Y, et al. A rapid and label-free platform for virus capture and identification from clinical samples. Proceedings of the National Academy of Sciences of the United States. 2020;117(2):895. https://search.ebscohost.com/login.aspx?direct=true&AuthType=shib&db=edsggo&AN=edsgcl.613341191&site=eds-live&scope=site&custid=s6281220. doi: 10.1073/pnas.1910113117.

63. S. Link and M. A. El-Sayed, "Spectral Properties and Relaxation Dynamics of Surface Plasmon Electronic Oscillations in Gold and Silver Nanodots and Nanorods," J. Phys. Chem. B 103.40, pp. 8410-426, 1990.

64. R. P. Kooyman, "Chapter 2: Physics of Surface Plasmon Resonance," in N.A., N.A., pp. 15-34.

65. Downes, Andrew & Elfick, Alistair. (2010). Raman Spectroscopy and Related Techniques in Biomedicine. Sensors (Basel, Switzerland). 10. 1871-89. 10.3390/s100301871.

66. B&W T. Raman vs SERS: What's the difference. https://bwtek.com/raman-vs-serswhats-the-difference/. Accessed 2/21/, 2021.

67. M. Fleischmann, P.J. Hendra, A.J. McQuillan, Raman spectra of pyridine adsorbed at a silver electrode, Chemical Physics Letters, Volume 26, Issue 2, 1974, Pages 163-166, ISSN 0009-2614, https://doi.org/10.1016/0009-2614(74)85388-1.

68. Localized Surface Plasmon Resonance Sensors, Kathryn M. Mayer and Jason H. Hafner, Chemical Reviews 2011 111 (6), 3828-3857, DOI: 10.1021/cr100313v

69. Eom G, Hwang A, Kim H, et al. Diagnosis of tamiflu-resistant influenza virus in human nasal fluid and saliva using surface-enhanced raman scattering. ACS Sens. 2019;4(9):2282-2287. https://search.ebscohost.com/login.aspx?direct=true&AuthType=shib&db=cmedm&AN=31407570&site=eds-live&scope=site&custid=s6281220. doi: 10.1021/acssensors.9b00697.

70. Jadhav SA, Biji P, Panthalingal MK, et al. Development of integrated microfluidic platform coupled with surface-enhanced raman spectroscopy for diagnosis of COVID-19. Med Hypotheses. 2021;146. https://search.ebscohost.com/login.aspx?direct=true&AuthType=shib&db=edselp&AN=S0306987720332473&site=eds-live&scope=site&custid=s6281220. doi: 10.1016/j.mehy.2020.110356.

71. Zhan L, Zhen SJ, Wan XY, Gao PF, Huang CZ. A sensitive surface-enhanced raman scattering enzyme-catalyzed immunoassay of respiratory syncytial virus. Talanta. 2016;148:308-312. https://search.ebscohost.com/login.aspx?direct=true&AuthType=shib&db=edselp&AN=S003991401530446X&site=eds-live&scope=site&custid=s6281220. doi: 10.1016/j.talanta.2015.10.081.

72. Busbee, B., Obare, S. and Murphy, C. (2003), An Improved Synthesis of High-Aspect-Ratio Gold Nanorods. Adv. Mater., 15: 414-416. https://doi.org/10.1002/adma.200390095

73. Liu S, Huang H, Woo C. Schwoebel-ehrlich barrier: From two to three dimensions. Appl Phys Lett. 2002;80(18):3295-3297.

74. Lagally MG, Zhang Z. Materials science: Thin-film cliffhanger. Nature. 2002;417(6892): 907-910.

75. Bradbury, Savile , Ford, Brian J. and Joy, David C.. "Scanning electron microscope". Encyclopedia Britannica, 30 Oct. 2019, https://www.britannica.com/technology/scanning-electron-microscope. Accessed 21 February 2021.

76. Károly Havancsák. High-resolution scanning electron microscopy. https://www.technoorg.hu/news-and-events/articles/high-resolution-scanning-electron-microscopy-1/]#. Updated 2018. Accessed 2/21/, 2021.

77. 1. Nack Center. NACK center: Advanced scanning probe microscopy. https://www.youtube.com/watch?v=T0w_xSH4CNA. Updated 2013. Accessed 2/21/, 2021.